

Schedule Adjustments and Control of Battery Energy Storage in Low-Voltage Distribution Networks



Maximilian J. Zangs
School of Built Environment
University of Reading

A thesis submitted for the degree of
Doctor of Philosophy in Electronic Engineering

2018

It is not a dream. It is a simple feat of scientific electrical engineering. Electric power can drive the world's machinery without the need of coal, oil or gas. Although perhaps humanity is not yet sufficiently advanced to be willingly lead by the inventors keen searching sense. Perhaps it is better in this present world of ours where a revolutionary idea may be hampered in its adolescence. All this that was great in the past was ridiculed, condemned, combatted, suppressed only to emerge all the more triumphantly from the struggle. [...] Our duty is to lay the foundation for those who are to come and to point the way. Yes humanity will advance with giant strides. We are whirling through endless space with an inconceivable speed. All around everything is spinning, everything is moving, everywhere there is energy.

— Nocola Tesla

Abstract

Declaration

I confirm that this is my own work and the use of all material from other sources has been properly and fully acknowledged.

Maximilian J. Zangs

Dedication

Acknowledgements

Contents

Abstract	ii
Declaration	iii
Acknowledgements	v
Table of Contents	vi
Table of Figures	ix
Abbreviations	xiv
Nomenclature	xvi
1 Introduction	1
1.1 Overview	1
1.2 Electrical Energy Storage	5
1.2.1 Energy Storage Technologies	7
1.2.2 Energy Storage Applications	8
1.3 New Thames Valley Vision	8
1.4 Problem Statement and Research Aim	8
1.5 Contribution	8
1.6 Publications	8

1.7	Thesis Structure	8
2	Literature Review of Storage Control	9
2.1	Overview	9
2.2	Background	10
2.2.1	Entity Management in Power Networks	10
2.2.2	Device Control Paradigms	10
2.3	Related Work	10
2.4	Energy Storage Control Methodologies	10
2.5	Summary of Gaps in Litearture	10
3	Improving operation performance of battery schedules at sub-half-hourly resolution	11
3.1	Overview	11
3.2	Key Network Parameters and Derived Cost Functions	13
3.2.1	Voltages at substation	16
3.2.2	Voltages at ESMU's PCC	18
3.2.3	Voltages at customer laterals	20
3.2.4	Total power flow	22
3.2.5	Substation line utilisation	25
3.2.6	Maximum line utilisation	26
3.2.7	Distribution losses	28
3.3	Network, Data and Battery Models	29
3.3.1	Standardised Network Model	29
3.3.2	Load Profiles: Minutely and Half-Hourly	29
3.3.3	Battery Model	32
3.4	Closed-Loop Optimisation Method	36
3.4.1	ESMU Schedule Generation	36

3.4.2	Closed-Loop Schedule Adjustment	39
3.4.3	Method Execution and Result Assessment Procedure	41
3.5	Results and Discussion	44
3.5.1	Time Series Analysis	44
3.5.2	Difference Analysis	51
3.5.3	Probability Density Analysis	55
3.6	Summary	55
4	Real-Time Adjustment of Battery Operation using MPC Guided Schedule Deviation	58
4.1	Overview	58
4.2	MPC and PID Control Design	60
4.3	Data and Power Forecast Acquisition	60
4.4	Method and Case Studies	60
4.5	Results and Discussion	60
4.6	Summary	60
5	Effects of Control Instruction Desynchronisation in a Distributed MAS of Smart-Charging Batteries	61
5.1	Overview	61
5.2	Summary	61
6	Cooperative Operation of Distributed Batteries without Communications Infrastructure Needs	62
6.1	Overview	62
6.2	Summary	62
7	Conclusion	63
7.1	Overview of Main Findings	63

7.2	Knowledge Contribution	63
7.3	Research Limits	63
7.4	Future Work	63
	Bibliography	64
	A Additional Results	68
A.1	Improving operation performance of battery schedules at sub-half-hourly resolution	68
A.1.1	Additional Time Series Analysis	68
A.1.2	Additional Difference Analysis	68
A.1.3	Probability Density Analysis	68
	B Multi-Agent Systems	86
B.1	FIPA Implementation	86
B.2	Communication Protocols	86
	C Stochastic EV Demand Model	87
	D Network Simulation Interface	88
D.1	OpenDSS	88
D.2	Java	88
D.3	MATLAB	88
D.4	Python	88

List of Figures

1.1	Annual residential demand for electricity from FES2016 [1]	3
1.2	“Gone Green” power demand comparison to 2013/14 by type (excluding losses) from FES2015 [2]	4
1.3	Energy storage applications and corresponding value for various discharge durations [3]	6
3.1	Benefit of using cost function over utility function	14
3.2	Cost function values for different substation voltages	18
3.3	Sketch of the benefits that occur when ESMU injects power into the feeder in order to mitigate the voltage drop along the cable	19
3.4	Voltage at the loads in the IEEE LV Test Case network for a total load of 440kVA against distance between the corresponding load and substation: for the quadratic fit $R^2 = 58.76\%$	21
3.5	Sample network imbalance for different phase loadings as defined in ANSI/NEMA MG 1-2011	24
3.6	Cost of line or fuse utilisation against network current	26
3.7	Losses against increasing power demand	28
3.8	A power flow plot of the IEEE-PES European Test Case Feeder, i.e. a LV distribution network in the UK.	30
3.9	Highly variable and volatile demand profile vs half-hourly demand (i.e. a forecast under perfect foresight conditions)	32

3.10	Flowchart to calculate the next SOC (i.e. $SOC(t+1)$) based on current ESMU power (i.e. $s_{ESMU}(t)$) and current SOC (i.e. $SOC(t)$)	35
3.11	Impact of half-hourly ESMU schedule on sub-half-hourly power profile	38
3.12	ESMU schedule adjustment flow diagram	40
3.13	Method execution and results assessment flowchart	42
3.14	Voltage level modifications as noted at the ESMU's PCC by adjusting its schedule	45
3.15	Voltage level improvements at all buses in the entire distribution network due to the ESMU schedule adjustment.	47
3.16	Reduction of the network's phase unbalance due to the adjustment of the ESMU schedule.	48
3.17	Neutral power reduction due to the ESMU schedule adjustments	49
3.18	Power factor cost improvements due to the adjustment of the ESMU schedule	50
3.19	Instantaneous losses of the distribution network when adjusting the ESMU schedule in order to reduce the former (energy lost: 75.9Wh for base; 74.7Wh for normal; 69.9Wh for minimised).	50
3.20	Improvement of the worst line utilisation across the entire network when adjusting the ESMU schedule correspondingly.	51
3.21	Cost-function improvement spread, when comparing against the normal ESMU operation case and when optimising for the underlying cost (a separate y-axis is introduced for the optimisation of “neutral power”).	52
3.22	<i>p</i> -values for null hypothesis test	56
A.1	Additional substation voltage level comparison between base, normal and the case where the ESMU's schedule was adjusted.	69
A.2	Additional ESMU voltage level comparison between base, normal and the case where the ESMU's schedule was adjusted.	70

A.3 Additional voltage level comparison between base, normal and the case where the ESMU's schedule was adjusted.	71
A.4 Additional phase unbalance cost comparison between base, normal and the case where the ESMU's schedule was adjusted.	72
A.5 Additional power factor cost comparison between base, normal and the case where the ESMU's schedule was adjusted.	73
A.6 Additional comparison of the substation fuse utilisation between base, normal and the case where the ESMU's schedule was adjusted.	74
A.7 Additional line utilisation comparison between base, normal and the case where the ESMU's schedule was adjusted.	75
A.8 Additional comparison of distribution loss cost between base, normal and the case where the ESMU's schedule was adjusted.	76
A.9 Cost difference spread, based on the ESMU schedule adjustment to minimise substation voltage deviation	77
A.10 Cost difference spread, based on the ESMU schedule adjustment to minimise ESMU's PCC voltage deviation	78
A.11 Cost difference spread, based on the ESMU schedule adjustment to minimise the maximum voltage deviation on any bus of the network .	79
A.12 Cost difference spread, based on the ESMU schedule adjustment to minimise the network's phase unbalance	80
A.13 Cost difference spread, based on the ESMU schedule adjustment to minimise the network's power flow in the neutral conductor	81
A.14 Cost difference spread, based on the ESMU schedule adjustment to minimise the network's offset to unity power factor	82
A.15 Cost difference spread, based on the ESMU schedule adjustment to minimise the substation's fuse utilisation	83

A.16 Cost difference spread, based on the ESMU schedule adjustment to minimise the maximum line utilisation of any line in the network . . .	84
A.17 Cost difference spread, based on the ESMU schedule adjustment to minimise distribution losses	85

Abbreviations

AR	Auto-Regressive
ARMAX	Auto-Regressive Moving-Average Exogenous
ARX	Auto-Regressive Exogenous
BES	Battery Energy Storage
BESS	Battery Energy Storage Solution
CAES	Compressed Air Energy Storage
DG	Distributed Generation
DNO	Distribution Network Operator
DOD	Depth of Discharge
DSM	Demand Side Management
DSR	Demand Side Response
EPRI	Electric Power Research Institute
ESMU	Energy Storage Management Unit
ESQCR	Electricity Supply Quality and Continuity Regulations
ESS	Energy Storage Solution
EV	Electric Vehicle
FCES	Fuel Cell driven Energy Storage
FIPA	Foundation for Intelligent Physical Agents
GB	Great Britain
JADE	Java Agent Development Environment
LCT	Low Carb on Technology
NARX	Nonlinear Auto-Regressive Exogenous
NTVV	New Thames Valley Vision
P2N	Phase to Neutral
P2P	Phase to Phase
PCC	Point of Common Coupling
PMU	Power Management Unit
PV	Photo Voltaic
SMU	Storage Management Unit
SSE-EN	Scottish and Southern Energy - Electricity Networks
SOC	State of Charge
SQP	Sequential Quadratic Programming
TES	Thermal Energy Storage
UK	United Kingdom
VPP	Virtual Power Plant

Nomenclature

α, β, γ	Three intermediary variables
$\Delta E_{battery}(t)$	Change in the battery's energy level at time t .
$\delta s_{ESMU,p}(t)$	Change or adjustment in ESMU's apparent power that is injected into phase p at time t .
$\Delta SOC(t)$	Change in the ESMU's SOC at time t .
η	Efficiency (e.g. round-trip efficiency of power converters in ESMU's PMU).
μ	Losses (e.g. self-discharge losses in a battery).
$UF(\mathbf{x})$	Unbalance Factor of a vector \mathbf{x} .
$\zeta_{\text{load voltage}}(v_{i,p})$	Voltage divergence cost for a single-phase customer voltage v at customer i , who is connected to phase p .
$\zeta_{\text{unbalance}}(\mathbf{s})$	Unbalance cost for a three-phase power vector \mathbf{s} where $s_p \in \mathbf{s}$.
$\zeta_{\text{voltage}}(v_p)$	Voltage divergence cost for a single-phase voltage v on phase p .
$C_{battery}$	Capacity of battery.
$E_{battery}(t)$	Energy stored in battery at time t .
I	Number of loads in the network model, here $I \in \mathbb{N}$.
i	Load number of a given load in the network model, here $i \in [1, 2, \dots, I]$.
$i_{line,l,p}(t)$	Single phase line current that is calculated for line l on phase p during time t .
L	Number of lines in the network model, here $L \in \mathbb{N}$.
l	Line number of a given line in the network model, here $l \in [1, 2, \dots, L]$.
p	Phase number, here $p \in \{1, 2, 3\}$.
$s_{battery}(t)$	The apparent power (with no reactive component) that is charged into or discharged from the battery at time t .

$s_{ESMU,p}(t)$	ESMU's apparent power that is injected into phase p at time t .
$s_{loss}(t)$	Computed network losses at time t .
$s_{network\ load}(t)$	Sub-half-hourly network load at time t .
$s_{network\ load}^*(t^*)$	Half-hourly (or coarse) network load at time t^* .
$s_{ss,p}(t)$	Single phase apparent power measured at substation for phase p at time t .
$SOC(t)$	Battery's state of charge at time t .
T	Number of steps of the entire power flow simulation, here $T \in \mathbb{N}$ (i.e. $T = 1440$ for one day of minutely simulations).
t	Time-step of the current simulation step, here $t \in [1, \dots, T]$.
T^*	Number of coarse simulation steps, here $T^* \in \mathbb{N}$ and $T = \alpha T^*$ where $\alpha \in \mathbb{N}$ (i.e. $T^* = 48$ for one day of half-hourly simulations).
t^*	Coarser time-step where one integer increment represents multiple integer increments in t , here $t^* \in [1, \dots, T^*]$.
t_s	Sample-period or iteration-duration used in the simulations, usually in seconds unless otherwise specified.
V_h	High-voltage threshold which is calculated from V_n , i.e. 254V P2N ($\approx V_n \times 1.1$)
V_l	Low-voltage threshold which is calculated from V_n , i.e. 245.7V P2N ($\approx V_n \times 0.94$)
V_n	Nominal voltage for a LV network, i.e. 230V P2N ($\approx \frac{400}{\sqrt{3}}\text{V}$).
$v_{ESMU,p}(t)$	Single phase voltage that is measured at the ESMU's PCC for phase p at time t .
$v_{load,i,p}(t)$	Single phase load voltage that is calculated for load i on phase p during time t .
$v_{ss,p}(t)$	Single phase voltage measured at the substation transformer's secondary winding for phase p at time t .
V_{ss}	Nominal voltage as measured at the substation transformer's secondary winding; for the IEEE LV Test Case the voltage is 254.6V P2N.

Chapter 1

Introduction

1.1 Overview

Today's society and its lifestyle are highly dependent on the continuous availability of energy. More specifically, electrical energy has experienced the most significant increase in demand. One reason behind this demand increase is due to the environmental aim to reduce green house gas emissions by 80% by 2050. Another reason is based on political agendas to reduce national dependence on fossil fuels like oil, coal and gas. Therefore, governments incentivised and subsidised the uptake of Low Carbon Technologies (LTCs). Ongoing electrification of heating and transport, as well as increased penetration of Distributed Generation (DG) are the results. Whilst the electricity grid's infrastructure was initially constructed to deliver electricity in a unidirectional manner, it may no longer be able to support the current energy trends. Conventional solutions are costly and disruptive network reinforcement. Instead, electrical energy storage is proposed to support the network operation and mitigate or defer network reinforcement [4, 5].

The demand for electricity in the United Kingdom (UK) has increased significantly over the past century, and reports suggest that this trend is going to continue.

National Grid, one of the big UK network operators, published their Future Energy Scenarios (FES), highlighting the challenges that are yet to come [2]. In this report, four scenarios have been identified, and National Grid explains them as follows (excerpts taken from FES [2]):

- “**Gone Green** is a world where green ambition is not restrained by financial limitations. New technologies are introduced and embraced by society, enabling all carbon and renewable targets to be met on time.”
- “**Slow Progression** is a world where slower economic growth restricts market conditions. Money that is available is spent focusing on low cost long-term solutions to achieve decarbonisation, albeit it later than the target dates.”
- “**No Progression** is a world focused on achieving security of supply at the lowest possible cost. With low economic growth, traditional sources of gas and electricity dominate, with little innovation affecting how we use energy.”
- “**Consumer Power** is a world of relative wealth, fast paced research and development and spending. Innovation is focused on meeting the needs of consumers, who focus on improving their quality of life.”

In Figure 1.1 the UK’s future residential electricity demand is plotted for each of the four scenarios. Here, despite a subtle dip towards a new low in demand during 2025, all scenarios show an increase in energy demand after 2025. Assuming that the UK is going to meet its environmental targets for 2050, National Grid’s “Gone Green” scenario may be the most likely.

In this case the total demand for electricity is predicted to significantly increase. This can be seen in Figure 1.2, where the change in national energy demand is compared against the current demand levels. Here, increased industry efficiency is foreseen to outweigh its demand for electricity, which is shown by an initially negative change

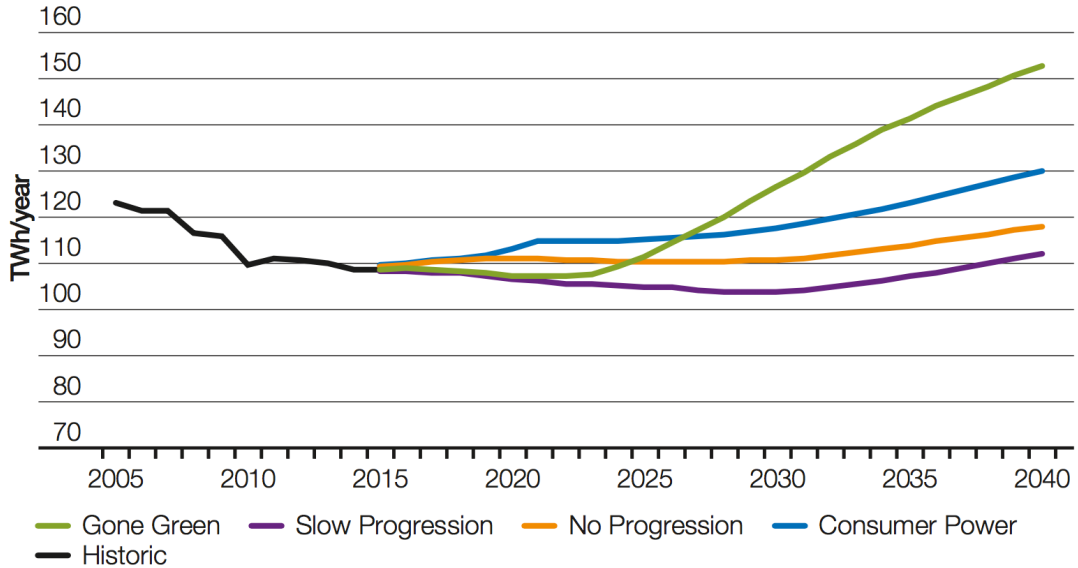


Figure 1.1: Annual residential demand for electricity from FES2016 [1]

in demand. Yet slower energy transitions in the private and commercial sector are foreseen to outweigh the industrial energy savings in 2025. Also, the ongoing uptake of sustainable technology will result in a further rise in annual residential demand, by nearly 50TWh in 2036. More than half of this residential demand, i.e. 27TWh, is expected to be caused by home charging of Electric Vehicles (EVs); which is the result of an expected 9.7 million EVs and Plug-in Hybrid EVs (PHEVs) being registered in the UK by 2040 [6]. This home charging will also have a significant impact on domestic peak power demand. In fact, it is expected to rise by as much as 6.5GW, predominantly because uncoordinated EV charging is feared to occur outside times of DG production [1].

The corresponding impact of this increased peak demand varies across the grid. For instance, the effect on the national transmission network's infrastructure is of little concern, since thermal limits are unlikely to be reached. Nonetheless, balancing demand and supply and controlling the grid's operating frequency are still key aspects that need to be considered. However, local power distribution networks are prone to thermal or voltage issues if peak demand is increased. One solution may be

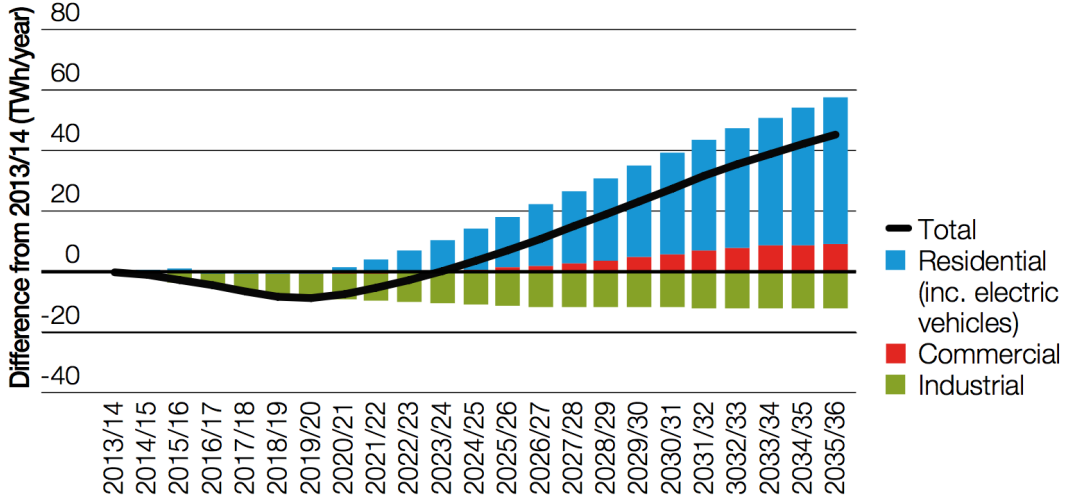


Figure 1.2: “Gone Green” power demand comparison to 2013/14 by type (excluding losses) from FES2015 [2]

the integration of Demand Side Response (DSM), where A study from 2010 shows that, as levels of EV and electric heating increase, equipment overloading becomes unavoidable unless devices are managed and coordinated intelligently [7]. In fact, the study suggests that in a Business as Usual (BaU) case, all transformers in distribution networks will overload when EV penetration reaches a level of 75%. This was shown to be the case for both areas of high demand density (i.e. $2\text{MVA}/\text{km}^2$) and low demand density (i.e. $0.5\text{MVA}/\text{km}^2$).

In the UK, Distribution Network Operators (DNOs) are the owners of the power distribution networks. Keeping this network within its operational constraints, e.g. preventing thermal overloads and voltage violations, used to be straight forward. For traditional reasons, energy is acquired in half-hourly chunks, but with the increasing electricity demand and associated power variation, estimating half-hourly demand becomes more difficult, and responding to sudden demand spikes becomes more difficult.

As already mentioned, electrical energy storage, the main focus of this research, has been identified as an valid alternative to conventional network reinforcements.

With the aforementioned challenges in mind, the author of this thesis focuses on the improved control of this storage to support the operation of the Low-Voltage (LV) power distribution network. More specifically, the question of how the important roles of electrical energy storage systems can be leveraged for both national and local benefits is addressed, and how their coordination is impacted by different external factors is researched. The remainder of this chapter explains the traditional and upcoming role of energy storage in the grid. Subsequent sections then introduce the UK distribution networks, the New Thames Valley Vision project and motivation of the author's work, the problem statement for the thesis, the novel contributions of this research and the structure of the thesis.

- Network issues including:

- Voltage deviation
- Phase unbalance
- Line utilisation
- Distribution losses

-

1.2 Electrical Energy Storage

The idea of using energy storage in the electricity grid has been discussed for quite some time, and its important role in future energy systems has already been identified in the 70s, i.e. Kalhammer [8]. As the name suggests, electrical energy storage systems have the ability to both consume, store, and release electrical energy by converting it into a different form of energy. Depending on the rate at which energy can be consumed and released, i.e. the system's power, as well as the amount of energy that can be stored, i.e. system's capacity, different functions can be provided. A study

for the Department Of Energy (DOE) showed that, when correctly exploited, these functions can yield direct financial benefits of \$157.56 billion over an estimated 10 year system lifecycle [9]. Figure 1.3 shows these benefits in relation to their typical discharge period, and links them to their associated functions, too. Here, Time Of Use (TOU) energy cost management yields the largest economic profit, yet from a historical point of view, bulk energy storage has played the most important role in the energy system. This kind of storage was used for large scale time-shifting and allowed the balancing of demand and supply without the need of ramping up or shutting down conventional power plants. Nowadays, this kind of storage can also tap into emerging revenue streams, i.e. to relieve network congestion, thus deferring the need for network reinforcement whilst allowing the integration of volatile renewable energy sources. So far, 127GW of bulk energy storage has been built worldwide [10], tripling it ever since Kalhammer's publication [11, 12].

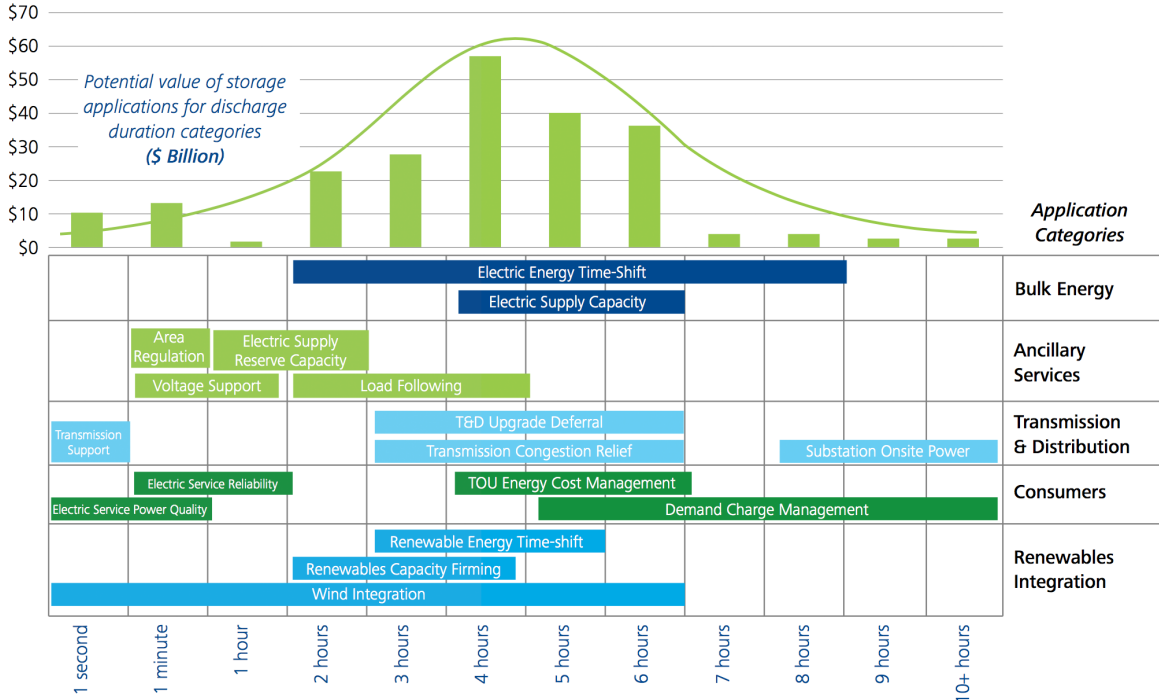


Figure 1.3: Energy storage applications and corresponding value for various discharge durations [3]

However, the scale and lack of responsiveness of such bulk energy storage systems

prevents them from being used in local distribution networks where fast system responses are required. Different energy storage technologies and their applications are briefly introduced in this section.

1.2.1 Energy Storage Technologies

The oldest form of grid scale energy storage, i.e. for bulk energy storage, is pumped hydro-electric energy storage. In 2012, 99% of bulk storage was comprised of pumped hydro [13]. Since pumped hydro is not a suitable technology for distribution network implementation, it is not considered in this technology assessment.

One of the first comprehensive reviews that included small- to medium-scale energy storage technologies was published by McLaren and Cairns [14]. They discussed electrochemical energy storage ^{*}, thermal energy storage [†], mechanical energy storage [‡], chemical energy storage [§], and magnetic energy storage [¶]. With subsequent advancements in technology, Battery Energy Storage Systems (BESS), Compressed Air Energy Storage Systems (CAESS) and Flywheel Energy Storage Systems (FESS) have become the most promising choices for deployment in distribution networks [15, 16, 17]. However, with no moving parts, the increasing energy density, and improved control systems, batteries are starting to outperform the competition. They can be deployed in ever decreasing form factors and are about to outlast their competition, too [18].

^{*}i.e. lead-acid batteries, iron/nickel-oxide batteries, zinc/chlorine batteries, zinc/bromine batteries, redox batteries, hydrogen/nickel oxide batteries, metal/air batteries, sodium/sulfur batteries, sodium/metal chloride batteries, lithium/iron sulfide batteries, and lithium/iron disulfide batteries

[†]i.e. aquifers, latent-heat storage systems, aqueous systems, salt hydrates, clathrates, molten salt systems, and more

[‡]pumped hydro-electric energy storage, compressed air energy storage, flywheel energy storage

[§]hydrogen generation, storage, transmission and utilisation

[¶]superconducting magnetic energy storage

1.2.2 Energy Storage Applications

1.3 New Thames Valley Vision

1.4 Problem Statement and Research Aim

1.5 Contribution

1.6 Publications

- M. J. Zangs, P. Adams, T. Yunusov, W. Holderbaum, and B. Potter, “Distributed Energy Storage Control for Dynamic Load Impact Mitigation,” Energies, vol. 9, no. 8, p. 647, Aug. 2016. doi: 10.3390/en9080647
- M. J. Zangs, T. Yunusov, W. Holderbaum and B. Potter, “On-line adjustment of battery schedules for supporting LV distribution network operation,” 2016 International Energy and Sustainability Conference (IESC), Cologne, 2016, pp. 1-6. doi: 10.1109/IESC.2016.7569485

1.7 Thesis Structure

Chapter 2

Literature Review of Storage Control

2.1 Overview

Technology advancements and increasing popularity of renewable energy sources, combined with government incentives to support their uptake, also lead to a significant rise in Distributed Energy Resources (DERs). Yet to allow DERs to be installed without significant negative impact on the local MV or LV networks, required functions that large scale power levelling systems could not provide. More specifically, fast response to counteract highly volatile loads or unpredictable and distributed DERs; e.g. home PV installations [19].

- Improvement approaches include:
 1. Utility maximisation (Pareto-Optimum and Nash-Equilibrium)
 2. Cost minimisation (least squares technique, statistical hypothesis test; i.e. Student's t -test)
- Cost minimisation

2.2 Background

2.2.1 Entity Management in Power Networks

2.2.2 Device Control Paradigms

2.3 Related Work

2.4 Energy Storage Control Methodologies

2.5 Summary of Gaps in Litearture

Chapter 3

Improving operation performance of battery schedules at sub-half-hourly resolution

M. J. Zangs, et.al., “On-line adjustment of battery schedules for supporting LV distribution network operation,” 2016 International Energy and Sustainability Conference (IESC), Cologne, Germany, 2016, pp. 1-6.

— Available: <http://dx.doi.org/10.1109/IESC.2016.7569485>

3.1 Overview

Since the increasing domestic demand for electric energy is expected to put significant strain on existing power distribution networks, DNOs have a binary choice to address this issue. Either they invest in substantial network reinforcement, resulting in unavoidable cost and service disruption, or alternative network support mechanisms need to be installed. As mentioned in the Introduction in Section 1.3, DNOs prefer the latter option since it yields long term flexibility at significantly lower cost; more specifically, SSE-EN decided to deploy ESMU in LV power distribution networks. To

operate the ESMU so that its promised battery's life expectancy is reached and operational constraints are not violated, scheduled operation was chosen. To reiterate, during the scheduled operation of a ESMU it consumes or injects power according to a preset plan, which changes at regular intervals. For historic reasons and compliance, this interval was chosen to be of 30 minutes or half-hourly period.

Resulting operation of the LV network is based upon two factors:

1. the underlying forecast that was used to generate the ESMU schedule, and
2. the network parameters used to quantify the improvements that were experienced by the network if the half-hourly schedule had been applied.

Our previous research focused on improving half-hourly network operation [20, 21]. Yet limiting performance parameters and the measure of success to a high level at half-hourly resolution does not effectively address and mitigate the negative impact of sub-half-hourly (i.e. minute by minute) variations in demand.

Therefore, in this chapter, a closed-loop optimisation method is proposed that adjusts a ESMU schedule in a sub-half-hourly manner in order to improve network operation whilst maintaining the same average power flow during the half-hourly period. Unlike previous work in the field, this approach guarantees the correct execution of the predetermined ESMU schedule, whilst allowing higher ESMU responsiveness to high resolution variations in power demand.

In order to investigate how network operation may be improved, several, commonly used parameters are summarised in a set of cost functions. Initially, these cost functions are minimised individually to inspect their resulting individual impact. Then, they are combined in an optimal manner using a weighted sum cost function, and the final improvement is analysed. For each optimisation approach, power flow simulations are run on a standardised UK power distribution feeder. Finally, to statistically determine that the proposed cost minimisation approach resulted in better

network performance, a one-tailed null hypothesis is formulated, and rejected with $p < 0.05$. The null hypothesis for this piece of work (i.e. the assumption to be rejected), is:

Adjusting an ESMU schedule based on sub-half-hourly measurements of key network parameters cannot significantly improve network operation.

The term “*network measurements*” and the correlated measure of “*improvement*” is explained in the next section. All data acquisition and the power network models used for this piece of work are shown next. Then, the closed-loop optimisation method is presented. All results are discussed and, in the last section, the null hypothesis rejection is summarised.

3.2 Key Network Parameters and Derived Cost Functions

In literature (see Chapter 2), two distinct approaches have emerged to quantitatively improve the performance of a system: either cost is reduced or utility is maximised. Both approaches rely on a mathematical explanation of underlying features that relate to performance of the system. To recap; utility functions are maximised since they explain how beneficial a system state is, whereas cost should be minimised since they entail a suboptimal system performance. The choice for this piece of work was to associate key network parameters to tailored cost functions, with the reason that a cost can be minimised to a finite value, i.e. zero. Utility maximisation on the other hand is a mathematically unbound problem that may reach a maximum, yet this maximum can only be approximated through game theoretic approaches like Pareto- or Nash-Optimality. In other words, solutions to a cost function where the resulting cost is zero, are by definition optimal solutions, whereas a utility functions can have multiple maxima where optimality classification of these solutions is inherently more

difficult. To illustrate this fact, an arbitrary utility function, $\zeta_u(x)$, and an arbitrary (and unrelated) cost function, $\zeta_c(x)$, have been plotted in Figures 3.1a and 3.1b, respectively.

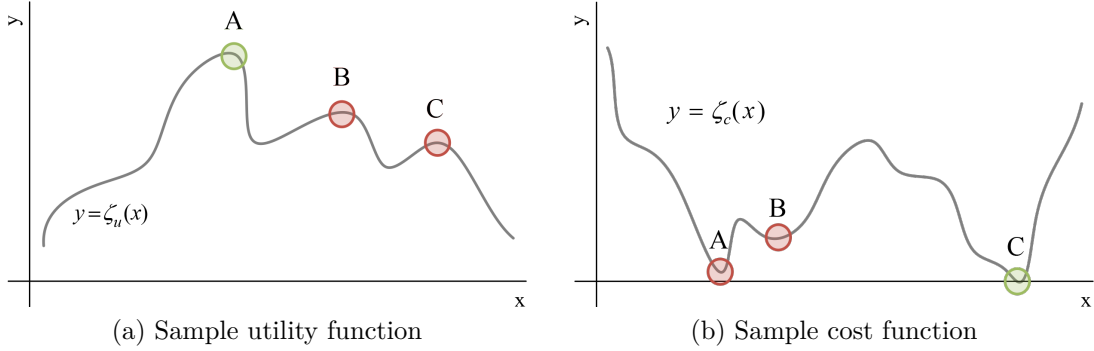


Figure 3.1: Benefit of using cost function over utility function

These two figures illustrate how the peaks of the utility function are at different, large values of y , and the troughs of the cost function tend towards zero. Both peaks or minima are found using solving algorithms; the most common mathematical solvers are the Gradient Descend Method, Newton-Raphson Method, and Active Set Method. If the cost or utility function is nonlinear or the system's gradient function can only be approximated more sophisticated algorithms had to be used, e.g. Mixed-Integer Linear Programming, Sequential Quadratic Programming (SQP), Genetic Algorithm, Particle Swarm Optimisation or the Interior Point Method. Depending on the starting conditions of those solvers, i.e. the initial values for x , different maxima or minima (i.e. points A , B or C) may be found. In the example above, the best solution for $\zeta_c(x)$ is at point A , whereas the best solution for $\zeta_u(x)$ is at point C . Whilst point A represents the highest utility, it is difficult to determine whether this maximum is a most optimal solution since utility is inherently unbounded, i.e. $\zeta_u(x) \in (-\infty, \infty) \forall x$. For the cost function on the other hand, point C represents an absolute minimum and optimal solution since the cost function's range is bounded to be greater or equal to zero, i.e. $\zeta_c(x) \geq 0 \forall x$. Therefore, the cost's proximity to zero can directly indicate the system performance (whilst a utility's proximity to infinity would not make sense).

With this in mind, the key network parameters are explained and the corresponding cost functions are defined next. The choice of parameters is virtually inexhaustible since one could treat every single current, voltage or phase angle as a potential indicator for network performance. In reality however (and particularly in the context of NTVV), a power distribution network can only be observed at a limited number of points. Here, these points were at the substation and the ESMU’s Point of Common Coupling (PCC). Therefore, all derived network parameters that are based on these measurements are treated as “realistic parameters”. It is however worth mentioning, that for the work presented in this chapter, all realistic parameters are extracted from power flow simulations.

In those simulations of power distribution networks (i.e. in OpenDSS), a system of equations that captures nodal power flow is solved. In the IEEE LV Test Case, there are 906 three phase buses, resulting in a total of 2718 nodes, for which complex currents and voltages can be obtained. This abundance of values means that a lot of additional parameters can be considered. Yet those parameters cannot easily be obtained in reality, which is why they are referred to as “theoretical parameters”. Due to the high abundance of these theoretical parameters, the impact of some of these parameters on network performance is quite limited. Therefore the set of theoretical parameters, that were used in this piece of work, was chosen based on their importance and impact on actual network operation.

A list of all realistic and theoretical key network parameters* is presented below.

- Voltages at substation transformer’s secondary winding
- Voltages at ESMU’s PCC
- Voltages at customer lateral[†]

*A key network parameter is marked with a dagger (\dagger) if it is a theoretical parameter that can only be extracted from power flow simulations.

- Total power flow
- Substation line utilisation
- Maximum line utilisation[†]
- Distribution losses[†]

In the following subsections, the formulation of all key network parameters' associated cost functions is presented.

3.2.1 Voltages at substation

In UK LV distribution networks, substations supply power to a feeding cable. These substations provide the link from MV distribution networks, which operates at 11kV P2P, to the LV distribution network, which operates at nominal 230V P2N (i.e. 400V P2P). If the substation transformer was an ideal transformer, then the voltage measured at its secondary winding would remain constant with changing load. In reality however, the internal losses (e.g. conductive losses and magnetic leakage) lead to a drop in voltage as load increases. Therefore, any deviation from the substation's nominal voltage may be an indicator of suboptimal network operation.

Let the substation voltage for a single phase voltage be defined as $v_{ss,p}(t)$, where p is the phase number and t the time at which the measurement was taken. Then the resulting substation voltage vector $\mathbf{v}_{ss}(t)$ (where $v_{ss,p}(t) \in \mathbf{v}_{ss}(t)$) can be fed into a deviation cost $\zeta_{\text{voltage}}(\mathbf{v}_{ss}(t))$ to assess the cost of substation overloading. This cost is defined for any voltage vector (here $\mathbf{v}(t)$) as:

$$\zeta_{\text{voltage}}(\mathbf{v}(t)) := \sum_{p=1}^P \begin{cases} \zeta_h(v_p(t)) & \text{if } V_{ss} \leq v_p \forall t \\ \zeta_l(v_p(t)) & \text{otherwise} \end{cases} \quad (3.1)$$

where $P \in \mathbb{N}$ s.t. $V_l < V_{ss} < V_h$

In this cost function, $\zeta_h(v)$ and $\zeta_l(v)$ are two functions that convert a single voltage value, i.e. v_p , into a normalised positive cost. If the voltage v_p is greater than or equal to the nominal substation voltage, V_{ss} , then the result from $\zeta_h(v)$ is used as a cost; otherwise the result from $\zeta_l(v)$ is used. In order to define these two functions, the corresponding high and low voltage thresholds, V_h and V_l respectively, need to be introduced. These two thresholds are based on the nominal LV voltage range of +10% -6% around V_n , i.e. 230V P2N.

$$\zeta_h(v) := \alpha \left| \frac{v - V_{ss}}{V_h - V_{ss}} \right|^\beta \quad (3.2)$$

$$\zeta_l(v) := \alpha \left| \frac{V_{ss} - v}{V_{ss} - V_l} \right|^\beta \quad (3.3)$$

In this context, α is the function's weight that linearly scales the cost function, and β regulates the function's offset gradient. More specifically, α determines the value of the cost functions for the values of V_l and V_h , and may take any value in $(0, \infty)$. For example, when $\alpha = 1$, then $\zeta_h(v_l) = 1$. β on the other hand may take any value in the range of $[2, \infty)$, to assure a continuously differentiable cost function. For this work, α and β were treated as constants and set to 1 and 2, respectively. Substituting these values into Equations 3.2 and 3.3, simplifies them to:

$$\zeta_h(v) := \left| \frac{v - V_{ss}}{V_h - V_{ss}} \right|^2 \quad (3.4)$$

$$\zeta_l(v) := \left| \frac{V_{ss} - v}{V_{ss} - V_l} \right|^2 \quad (3.5)$$

Since voltage levels drop continuously along a purely consumptive feeder, substations may boost the voltage above the nominal LV voltage level, yet keep it below the upper voltage threshold. The behaviour of boosting V_{ss} on the cost function $\zeta_{\text{voltage}}(\mathbf{v})$ is shown below (here $P = 1$).

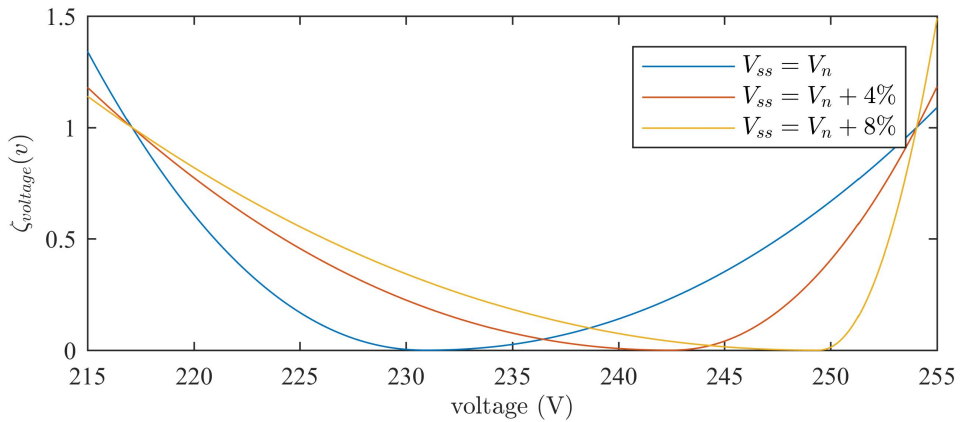


Figure 3.2: Cost function values for different substation voltages

It can be seen that the cost at the high and low voltage thresholds equates to one, and to zero at the set substation voltage. When boosting this voltage, V_{ss} , only the zero intersection is moved, whereas the high and low voltage crossings remain unchanged. In Figure 3.2, this behaviour is demonstrated by boosting V_{ss} by +4% and +8%.

3.2.2 Voltages at ESMU's PCC

At the ESMU's PCC, it is connected to all three phases of the feeding cable. The location of this PCC is at some distance from the substation or simply “down stream” the feeder. Where to connect the ESMU, in order to achieve a best possible network impact, is explained in Section 3.3. Ignoring the exact ESMU location, voltage along the line, i.e. from the substation to its PCC, will change and most likely drop. The

reason behind this effect is due to resistive and inductive losses in the distribution lines. These losses are amplified with proximity to the substation, since load currents are aggregated. For purely consumptive loads, and particularly under heavy load conditions, this voltage may at some stage drop below the low-voltage threshold. As mentioned in literature, this threshold is an operational constraint of LV networks and must not be violated to assure correct appliance operation and prevent financial penalisation.

In order to mitigate this voltage drop, power is injected into the feeder at the ESMU's PCC. Doing so boosts the voltage at that location since the portion of the load current that would normally be supplied by the substation is now delivered by the ESMU. The effect of this power injection is sketched in the figure below.

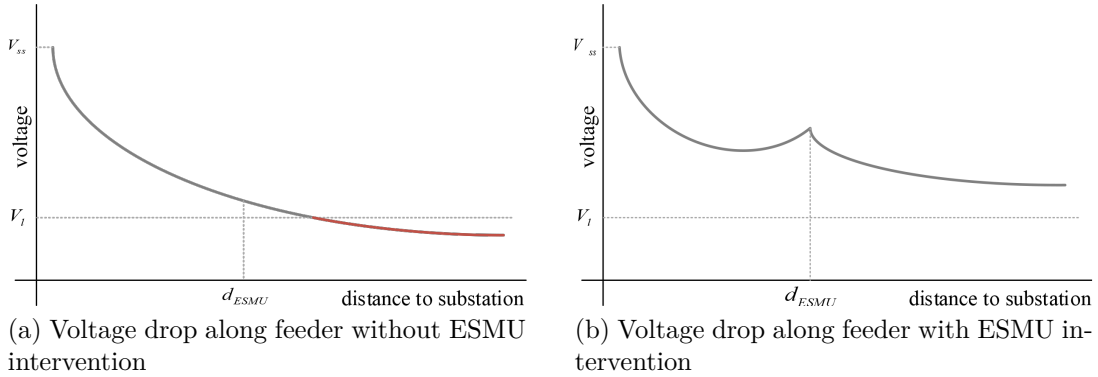


Figure 3.3: Sketch of the benefits that occur when ESMU injects power into the feeder in order to mitigate the voltage drop along the cable

In Figure 3.3a, an expected voltage drop along the feeder is sketched, where the downstream feeder section's voltage dropped below V_l . In contrast, Figure 3.3b shows how the ESMU's intervention can alleviate some load and raise the trailing voltage levels to a level above V_l .

This realistic key network parameter is translated into a cost function, since the P2N voltage at the ESMU's PCC can be measured quite easily. To do so, the three-phase PCC voltage, $\mathbf{v}_{ESMU}(t)$ (where $v_{ESMU,p}(t) \in \mathbf{v}_{ESMU}(t)$), is used in Equation 3.1; the same cost used for the substation transformer's secondary voltage. Therefore,

the resulting cost can be formulated as $\zeta_{\text{voltage}}(\mathbf{v}_{ESMU}(t))$.

3.2.3 Voltages at customer laterals

As mentioned in Chapter 1.1, the allowable voltage range at customers is defined by the Electricity Safety, Quality and Continuity Regulations (ESQCR). Monitoring those voltages in real-time to assure they obey these regulations is costly, and therefore they are left unmonitored. Ultimately, when it comes to voltage level correction, only substation voltage levels and customer voltage levels need to be controlled. This fact is to assure proper transformer operation (e.g. to maximise its lifespan) and to prevent penalisation due to customer voltage violation (i.e. fining according to the ESQCR). As explained in Section 3.2.2, ESMU can impact voltage levels for all customers but, as mentioned above, these voltage levels cannot be measured in reality. In simulations however, all loads' voltages can be extracted with ease, which is why they are included but treated as theoretical key network parameters.

To illustrate this load voltage drop, a snapshot OpenDSS simulation was run on the IEEE LV Test Case with all load powers set to a high value of 8kW*. In the following plot, the magnitude of the load bus voltages against the distance between the corresponding load and its feeding substation was drawn.

In this Figure 3.4, two observations can be made. For one, it can be seen that phases are significantly unbalanced. Secondly, customers further than 200m from the substation experience low-voltage events (for this particular scenario). As already proposed in the previous section, ESMU aims to avoid these voltage violations, but the number of loads would add significant computational burden on the any used solving algorithm.

To address this problem, the previously defined voltage cost function (i.e. Equa-

*Whilst historic and recent loads may reach values of this magnitude quite seldom, future customer demand with the aggregated effect home-charging of EVs may indeed yield extreme scenarios like this.

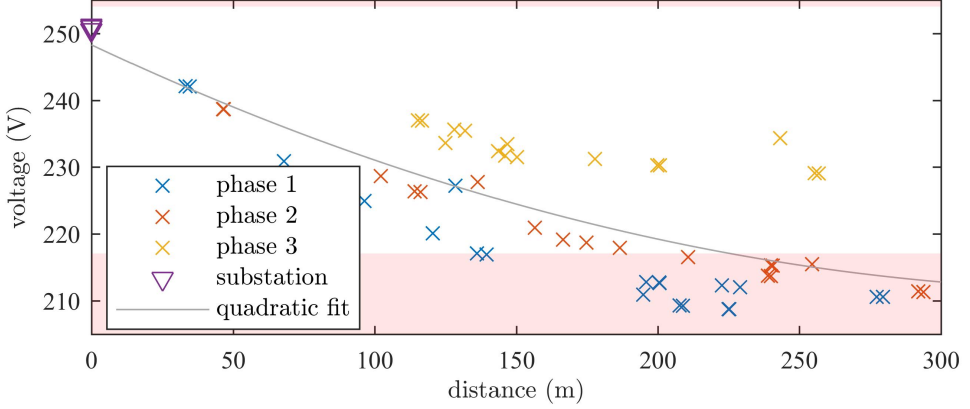


Figure 3.4: Voltage at the loads in the IEEE LV Test Case network for a total load of 440kVA against distance between the corresponding load and substation: for the quadratic fit $R^2 = 58.76\%$

tion 3.1) is expanded. Rather than including the cost for every single customer's voltage deviation, only the worst deviation is used. By limiting this number, solvers need not consider such a large number of parameters and only focus on the worst network parameter. This focus is of particular need if the impact of the ESMU on some customers' voltages is relatively low, since the aggregate cost would otherwise cloud the impact on those individual voltages. For this work, the customer (or load) voltage is defined as $\mathbf{v}_{load}(t)$ (where $v_{load,i,p} \in \mathbf{v}_{load}$) and used in the new cost function, $\zeta_{\text{load voltage}}(\mathbf{v}_{load}(t))$, as such:

$$\zeta_{\text{load voltage}}(\mathbf{v}(t)) := \max_{i,p} \zeta_{\text{voltage}}(v_{i,p}(t)) \forall t \quad (3.6)$$

where $i \in [1, \dots, I]$ and $p \in [1, \dots, P]$ and $P \in \mathbb{N}$

Here, i represents the customer number out of a total customer count I , and p the phases to which the customer is connected out of a total phase count P .

3.2.4 Total power flow

Beside having to keep voltages within their specified operational boundaries, DNOs want to make sure that the distribution network operates in an efficient and ideal manner. Determining how ideal a three-phase network operates can be done by e.g. assessing the balance of the network's phases. The frequently neglected disturbance of unbalanced phases may not have an immediately associated impact on the network's customers, but the negative long term effects (e.g. asymmetric load on transformers, rotating machines and increased neutral current) must be addressed since they weaken the network's infrastructure.

The choice of how customers are connected to LV feeders in the UK makes phase unbalance a more dominant problem than one might have thought. Customers in urban UK distribution networks have a single-phase link to the three-phase feeder line. The link is established by connecting their supply cables or "laterals" between a phase and the neutral conductor. In the UK, the phase allocation for each customer has been random, in order to distribute load as evenly as possible across all three phases. In theory, this approach should assure a more or less balanced three-phase load, yet in reality this is not the case. Even if the number of customers on each phase was the same for all three phases, the probability that all customers' load profiles are identical is very low. Therefore, the likeliness of LV distribution feeders in the UK to be unbalanced is very high.

Since substation monitoring is capable of providing three-phase power measurements, they are used as realistic key network parameters, and summarised in a sub-station power vector $\mathbf{s}_{ss}(t)$. Deriving phase unbalance from these three-phase sub is done by following the American National Standards Institute (ANSI) definition of phase unbalance [22]. The standardised Unbalance Factor (UF) is defined as:

$$\text{UF}(\mathbf{x}) := \frac{\max_n |\bar{\mathbf{x}} - x_n|}{\bar{\mathbf{x}}} \quad \text{where } x_n \in \mathbf{x} \quad (3.7)$$

and $n \in [1, \dots, N]$ and $N \in \mathbb{N}$

Here, \mathbf{x} can be an arbitrary vector, consisting of scalar values x_n (e.g. x_n may be voltage, current or power measurement per phase n), and for this work, x_n was chosen to be the power flow into one of the network's phases. For clarity, the notation of $\bar{\mathbf{x}}$ is used to define the mean of the given vector, i.e.:

$$\bar{\mathbf{x}} := \frac{1}{N} \sum_n^N x_i \quad (3.8)$$

From the substation monitoring, a three-phase substation power vector, $\mathbf{s}_{ss}(t)$ (where $s_{ss,p} \in \mathbf{s}_{ss}$), is used and the network's phase unbalance can be calculated. Since this forms another realistic key network parameter, the UF in Equation 3.7 was formulated into a cost function, too. The resulting cost function $\zeta_{\text{unbalance}}(\mathbf{s}_{ss})$ is defined as:

$$\begin{aligned} \zeta_{\text{unbalance}}(\mathbf{s}(t)) &:= \text{UF}(\mathbf{s}(t)) - 1 \forall t \\ &= \frac{\max_p \left| \overline{\mathbf{s}(t)} - s_p(t) \right|}{\overline{\mathbf{s}(t)}} \forall t \\ &= \frac{\max_p \left| \left(\frac{1}{P} \sum_p^P s_p(t) \right) - s_p(t) \right|}{\frac{1}{P} \sum_p^P s_p(t)} \forall t \end{aligned} \quad (3.9)$$

where $p \in [1, 2, \dots, P]$

The minimum value of $\text{UF}(\mathbf{s}_{ss})$ is one. Therefore an adjustment was required so that a perfectly balance network would result in an $\text{UF}(\mathbf{s}_{ss})$ of zero. An illustration how this cost function is provided in the Figure 3.5, as shown below.

Here, it can be seen how $\zeta_{\text{unbalance}}(\mathbf{s})$ varies with an increasing separation of the

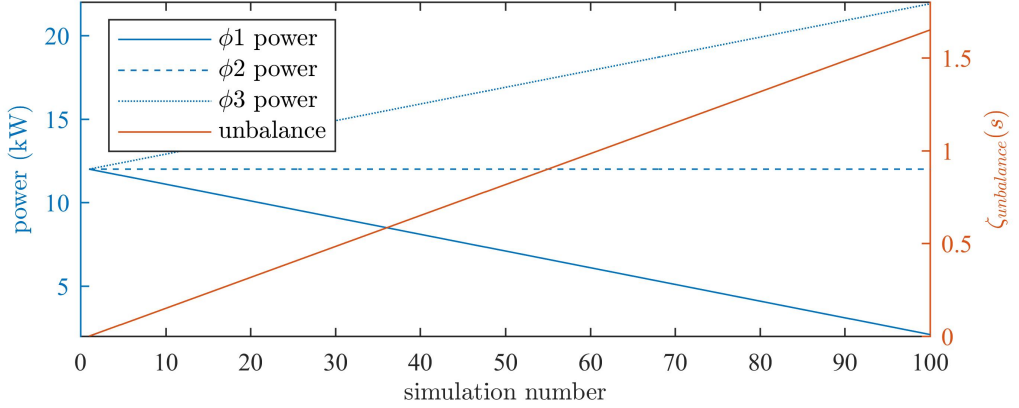


Figure 3.5: Sample network imbalance for different phase loadings as defined in ANSI/NEMA MG 1-2011

three phases' power values.

Additionally, to assess the effective utilisation of the power distribution network, the Power Factor (PF) divergence is also addressed. PF is the ratio between the supplied active and apparent power. It therefore gives an indication of how much “good”* power is being consumed by the system. Experts would agree that keeping the PF of a system close to unity indicates that the system only draws active power and therefore is using the least amount of power transmission resources. In order to assess the proximity to unity PF a PF cost function, $\zeta_{PF}(\mathbf{s}_{ss}(t))$, is defined a power vector as input:

$$\zeta_{PF}(\mathbf{s}(t)) := \sum_{p=1}^P \frac{\operatorname{Re}(s_p(t))}{|s_p(t)|} - 1 \forall t \text{ where } s_p(t) \in \mathbf{s}(t) \text{ and } P \in \mathbb{N} \quad (3.10)$$

Here, deviating from a unity PF per phase increases the associated cost, whilst achieving a perfect PF for each phase results in a total cost of zero.

Lastly, the already mentioned neutral current is also a result of both three-phase unbalance and non-unity PF. Since all three phases are 120° out of phase, the sum

*Reactive power is used to maintain magnetic fields in rotating machines, yet this can be supplied by local reactive power compensators and thus need not occupy otherwise free power transmission resources.

of instantaneous powers should equate to zero. This would result in no neutral current flowing in the system. However, in an unbalanced system the power transmitted through the neutral conductor deviates significantly from zero. This situation is amplified since power distribution cables often use neutral conductors with significantly smaller diameter than those conductors used for the lines. Therefore, any additional power flow in this neutral conductor will deviate neutral voltages from zero volts and it could also exhaust the conductor's power carrying capacity, making the system more prone to failures. To address this last point, and before dealing with line utilisation, a final cost function that deals with the neutral loading $\zeta_{neutral\ load}(\mathbf{s}_{ss}(t))$ is defined as follows:

$$\zeta_{neutral\ load}(\mathbf{s}(t)) := \left| \sum_{p=1}^P s_p(t) e^{\frac{j2p\pi}{P}} \right| \forall t \text{ where } s_p(t) \in \mathbf{s}(t) \text{ and } P \in \mathbb{N} \quad (3.11)$$

For $\zeta_{neutral\ load}(\mathbf{s}_{ss}(t))$, each phase power, $s_{ss,p}(t)$, is therefore rotated by an integer multiple of 120° before adding them to obtain the neutral load vector. The magnitude of this apparent power vector is the size of the load in the neutral conductor.

3.2.5 Substation line utilisation

Although phase unbalance deteriorates the efficiency and life expectancy of three-phase network assets, high power demand puts strain on the physical cables themselves. This is due dominantly due to resistive and inductive losses heating the cables, and bringing them closer to their operational limits. Therefore, cables have an assigned thermal rating which must not be exceeded to prevent permanent cable damage or network failures. At substation level, to prevent over-currents, fuses or reclosers are installed that will disconnect the network under fault or high demand conditions. To quantify whether the substation fuse is approaching its tripping point, its nominal

rating is used as reference.

For the context of this work, this nominal fuse rating, i_{fuse} , is a fixed value for the fuse at the substation and must not be exceeded. Using the three-phase current vector from substation monitoring, $\mathbf{i}_{ss}(t)$ (where $i_{ss,p}(i) \in \mathbf{i}_{ss}(t)$) a cost function, $\zeta_{\text{fuse utilisation}}(\mathbf{i}_{ss}(t))$, can be defined as follows:

$$\zeta_{\text{fuse utilisation}}(\mathbf{i}(t)) := \left| \frac{\sum_{p=1}^P i_p(t)}{i_{fuse}} \right|^2 \quad \forall t \text{ where } p \in [1, \dots, P] \text{ and } P \in \mathbb{N} \quad (3.12)$$

A plot has been included in the below figure, which illustrates how this quadratic cost behaves as substation current increases.

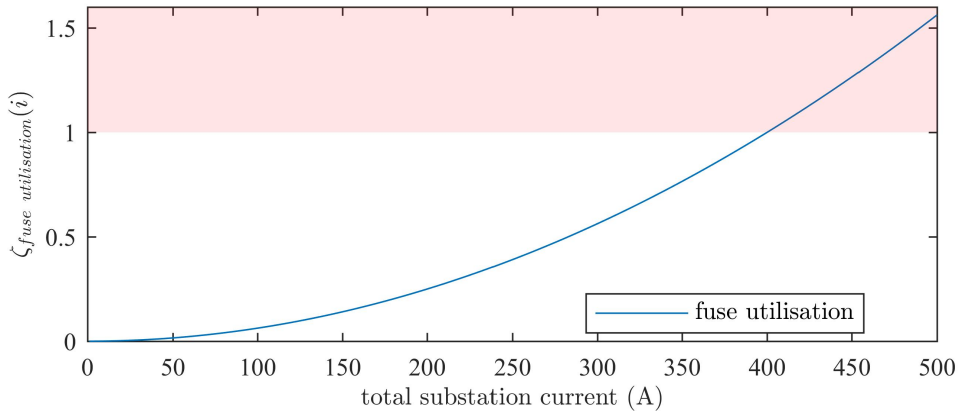


Figure 3.6: Cost of line or fuse utilisation against network current

For this simple case, the substation line rating was set as $i_{fuse} = 400\text{A}$, and the total substation current is the sum of all three phase currents.

3.2.6 Maximum line utilisation

Similar how voltage levels at all customers are theoretical key network parameters, currents in all lines are key network parameters, too. Optimising the aforementioned current at substation level would prevent unintentional feeder disconnection

and equipment damage, yet lines' ratings impose distributed limits, too. Moreover, as feeder cables are not of a singly type of cable. For instance, the main three-phase wire must to be sufficiently scaled to deliver several 100s of Amperes to a collection of customers, whilst branches with a few loads may only experience 10s of Amperes worth of current. Furthermore, as distance to the substation increases, fewer customers are connected down stream, which allows the feeding cables to be down scaled, too. This network topology is very common for radial distribution networks, since it saves significant equipment cost without compromising the network integrity. Yet with the advent of DG and electrified LTCs, the feeder's branches are going to experience larger current flows.

This is why the previous cost function, as it was defined in Equation 3.12, ought to be expanded to take all line currents and ratings into account. Since this work was based on network simulations, each line current, $i_{line,l,p}(t)$ (where l represents the line number and p the phase in that line), could be extracted with ease. Collecting them in $\mathbf{i}_{line}(t)$ (where $i_{line,l,p}(t) \in \mathbf{i}_{line}(t)$) allows the formulation of an extended line utilisation cost function, $\zeta_{\text{line utilisation}}(\mathbf{i}_{line}(t))$, which is defined as:

$$\zeta_{\text{line utilisation}}(\mathbf{i}(t)) := \max_l \left| \frac{\sum_{p=1}^P i_{l,p}(t)}{i_{nom,l}} \right|^2 \quad \forall t \text{ where } l \in [1, \dots, L] \quad (3.13)$$

$$\text{and } p \in [1, \dots, P] \text{ and } L \in \mathbb{N} \text{ and } P \in \mathbb{N}$$

In this quadratic cost function, $i_{nom,l}$ is the nominal rating of line l in the network. Also, and similar to Equation 3.6, by considering only the maximum line utilisation, computational burden is reduced whilst parameter dependent sensitivity is increased.

3.2.7 Distribution losses

When it comes to profit margins, energy losses in a distribution network are unwanted, since nobody pays for undelivered energy. Although the losses in a single distribution network are small in comparison to the losses in the entire electricity grid, the aggregate effect of reducing those losses could have a noticeable impact. To put this into perspective, the losses in the IEEE LV Test Case network were 58kW, when simulated under the same high demand scenario which was used for voltage drop visualisation in Section 3.2.3. This equates to 12% of the total network demand (i.e. $\frac{s_{losses}(t)}{\sum_{p=1}^P s_{ss,p}(t)} \approx \frac{58kW}{484kW}$). Since this is a high network load, losses would be noticeably lower for normal network operation. This is made apparent in Figure 3.7, where the uniform network load is varied and the corresponding losses are plotted against this variation.

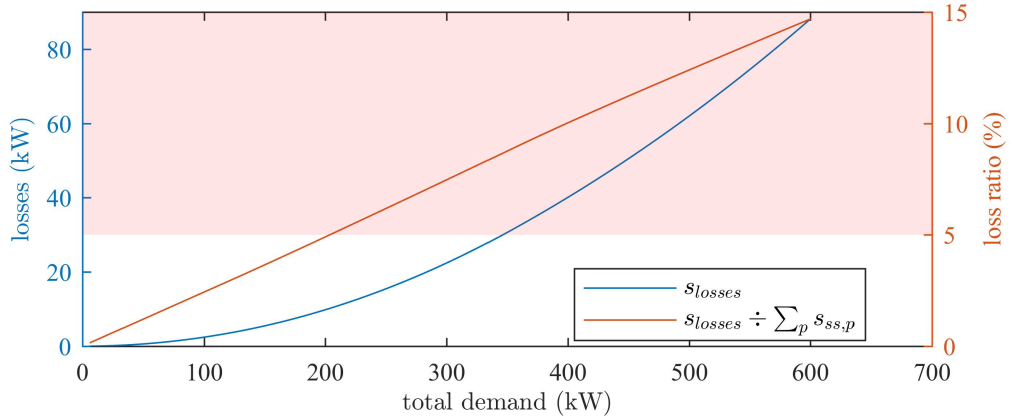


Figure 3.7: Losses against increasing power demand

In Figure 3.7, the region where losses exceed 5% of the total network power is highlighted in red. These preliminary results were found from power flow simulations. In reality however, losses cannot be determined this easily. Therefore, the network losses, $s_{losses}(t)$, are seen as theoretical key network parameters and used in the final cost function $\zeta_{losses}(s_{losses}(t))$, which is simply defined as:

$$\zeta_{\text{losses}}(s(t)) := |s(t)| \forall t \quad (3.14)$$

3.3 Network, Data and Battery Models

All key network parameters and their associated cost functions have now been established. In this section the network model and power flow simulation, from which all aforementioned key network parameters were extracted is explained. Also, all data that is used throughout the research, as it is presented in this chapter, is included presented, too.

3.3.1 Standardised Network Model

The IEEE Power and Energy Society (IEEE-PES) provided several multi-node test feeder cases. These test cases used to be limited to distribution networks in the United States. In 2015 however, they published a standardised model of a LV distribution network for the UK power network. This model is called the “European Low Voltage Test Feeder” and an OpenDSS compatible version can be obtained from their website, too [23]. Within the context of this work, the feeder is referred to as the “LV Test Case” and a network plot of this feeder has been included for reference.

Here, a substation (triangle in north west) provides power to the feeder, and the amount of power is visualised by using a thicker line plot. There are 55 single-phase households connected to the substation and for this particularly case, are each customer drew 2kW.

3.3.2 Load Profiles: Minutely and Half-Hourly

Alongside the LV Test Case, 100 minutely demand profiles were supplied; each being 24h long. Therefore, by assigning one load profile to each customer, a series of 1440

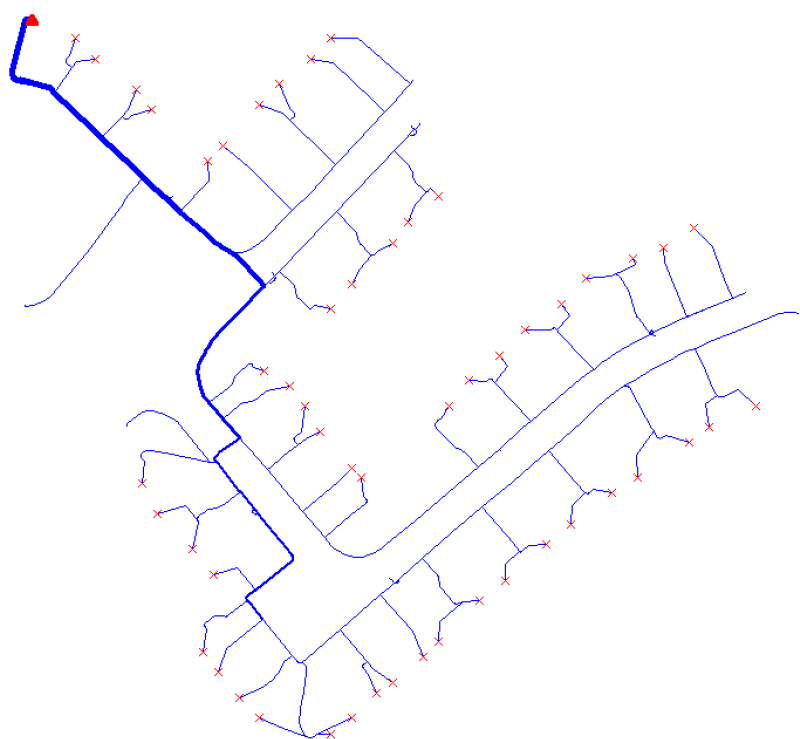


Figure 3.8: A power flow plot of the IEEE-PES European Test Case Feeder, i.e. a LV distribution network in the UK.

snapshot simulations could be run in OpenDSS in order to simulate the variation and volatility in demand over an entire day. Since the provided power values are only of active power, a standardised power factor of 95% was assumed for all loads to calculate their reactive component. This non-unity power factor simulates a certain inductive load, which would otherwise be neglected.

Computing the ESMU schedule at minutely resolution, or any sub-half-hourly resolution, is very computationally demanding and highly ineffective since cutting edge power forecasts have only now reached half-hourly resolution. Therefore, the sub-half-hourly profile must be down-sampled or extrapolated to a coarser resolution. This extrapolation is achieved by first calculating the total daily demand profile at sub-half-hourly resolution, i.e. $s_{\text{network load}}(t)$:

$$s_{\text{network load}}(t) := \sum_{i=1}^I s_{\text{load},i}(t) \quad (3.15)$$

Then, the day is split into a number of half-hourly time-slots, T^* , and the average power was computed over each of those time-slots. It is worth mentioning, that the number of time-slots for the sub-half-hourly load profile, T , must be divisible by the number of time-slots for the half-hourly (or coarser) profile T^* ; i.e. $T \stackrel{!}{=} \alpha T^*$ where $\alpha \in \mathbb{N}$. The resulting half-hourly network load, $s_{\text{network load}}(t^*)$, is thus extrapolated as follows:

$$s_{\text{network load}}^*(t^*) = \frac{T^*}{T} \sum_{t=1}^{\frac{T}{T^*}} s_{\text{network load}} \left(\frac{T}{T^*}(t^* - 1) + t \right) \forall t^* \text{ where } t^* \in [1, \dots, T^*] \quad (3.16)$$

It is worth mentioning, that from here on, all subsequent cost functions that deal with half-hourly profile shapes, are annotated as variations ζ^* , whilst sub-half-hourly or real-time costs are annotated as variations of ζ . This difference will become important when differentiating between scheduling costs and the aforementioned network

costs (which are based on a set of key network parameters). Nonetheless, to illustrate how the original sub-half-hourly network load is extrapolated into the resulting half-hourly demand, both are plotted in a figure below.

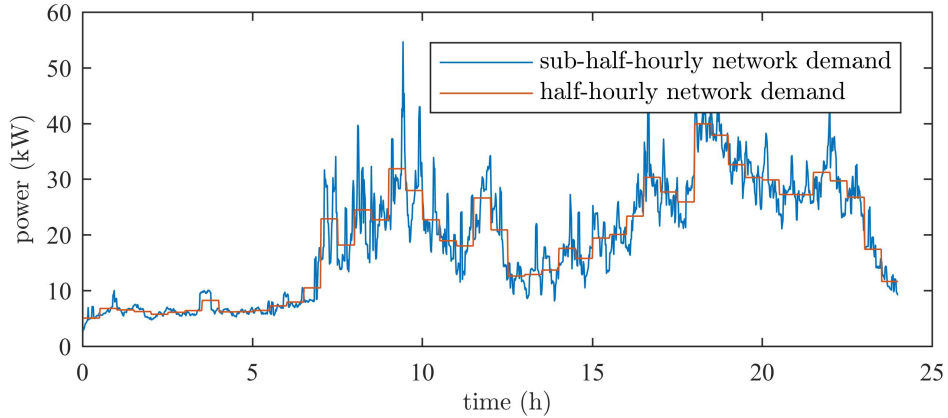


Figure 3.9: Highly variable and volatile demand profile vs half-hourly demand (i.e. a forecast under perfect foresight conditions)

Here, in Figure 3.9, it can be observed how the high variability and volatility in power is removed in the half-hourly profile. When generating the ESMU schedules (which is addressed in Section 3.4.1) these variations are neglected and the unwanted peak power demands are hence no longer sufficiently compensated.

3.3.3 Battery Model

The deployed ESMU systems themselves consist of two parts: the Power Management Unit (PMU) and the Energy Storage Unit (ESU). The PMU controls the phase powers converters and links the battery packs to the grid. Each PMU's power rating, S_{rating} , is the maximum phase power of 12kVA and, beside battery charging and discharging, can also perform filtering functions, e.g. compensating for harmonic distortion. The ESU is a modular container of 12.5kWh of Li-Ion energy storage, that can be aggregated to increase the energy storage capacity. All battery monitoring, conditioning and regulation is performed internally and need not be considered for

the scope of this work. However, control instructions that are sent to the ESMU system itself must not request the device to operate outside its own specifications.

In order to simulate this ESMU system and its energy flow behaviour, a model had to be derived from the given device specifications. This model includes both an inversely proportional charge-discharge efficiency, and a standby loss. The charge-discharge efficiency is related to the efficiency of the PMU's power converters, which are quoted to have a round trip efficiency of 98%. The standby loss on the other hand is associated to the nominal control system's power demand as well as the battery's self-discharge rate. It has become common practice to assess an energy storage's charge level as the State of Charge (SOC). This SOC is described as:

$$SOC(t) := \frac{E_{battery}(t)}{C_{battery}} \forall t \quad (3.17)$$

Here, the SOC is defined for any given time t , as the actual energy stored in the ESU, $E_{battery}(t)$, divided by the capacity of the system, $C_{battery}$. With the conversion efficiency as the factor η , the battery charge and discharge power, $s_{battery}(t)$ (in kW)*, can be calculated for any given ESMU power, $\mathbf{s}_{ESMU}(t)$ (where $s_{ESMU,p}(t) \in \mathbf{s}_{ESMU}(t)$).

$$s_{battery}(t) = \begin{cases} \eta \operatorname{Re} \left\{ \sum_{p=1}^P s_{ESMU,p}(t) \right\} & \text{if } \sum_{p=1}^P s_{ESMU,p}(t) \geq 0 \\ \frac{1}{\eta} \operatorname{Re} \left\{ \sum_{p=1}^P s_{ESMU,p}(t) \right\} & \text{otherwise} \end{cases} \quad \forall t \text{ and } P \in \mathbb{N} \quad (3.18)$$

Although the ESMU's PSU rating, S_{rating} , may allow for a maximum power consumption of 36kVA (i.e. $= 3 \times 12\text{kVA}$), the charging power is limited based on a charging factor, C_{factor} , which was chosen to be the standard value of 1.6. This factor is the ratio between the battery's maximum discharge power and its total capacity

*It is worth mentioning, that s is chosen for apparent power (i.e. active and reactive power in kVA), yet $s_{battery}$ is purely active (i.e. in kW).

(i.e. $s_{battery}(t) \leq C_{factor} \times C_{battery} \forall t$). Assuming this charge/discharge power is applied and constant during a sample period of t_s , an equation for the optimum change in stored energy can be formulated.

$$\Delta E_{battery}(t) = s_{battery}(t)t_s \forall t \quad (3.19)$$

As already mentioned, the energy level is however affected by standby losses, which are captured by a self-discharge factor, μ . Therefore, when adding the change in energy level to the current energy level, in order to calculate the next energy level, this factor needs to be taken into account.

$$E_{battery}(t+1) = \mu(\Delta E_{battery}(t) + E_{battery}(t)) \quad (3.20)$$

In an ideal case, $\mu = 1$, where no energy would be lost in the storage system. Finally, by adding the current energy level to the change in energy level, and by substituting Equation 3.17, the next SOC can be found:

$$SOC(t+1) = \mu \left(\frac{s_{battery}(t)t_s}{C_{battery}} + SOC(t) \right) \forall t \quad (3.21)$$

A flowchart to visually capture the model, as it is explained from Equation 3.17 to 3.21, is presented below.

Here, all green and blue fields indicate, respectively, model inputs and results. The white states represent operations applied onto those inputs and results and in the end yield the output, i.e. the yellow field.

[†]In the flowchart “charging” implies that $\sum_{p=1}^P s_{ESMU,p}(t) \geq 0$ as explained in Equation 3.18.

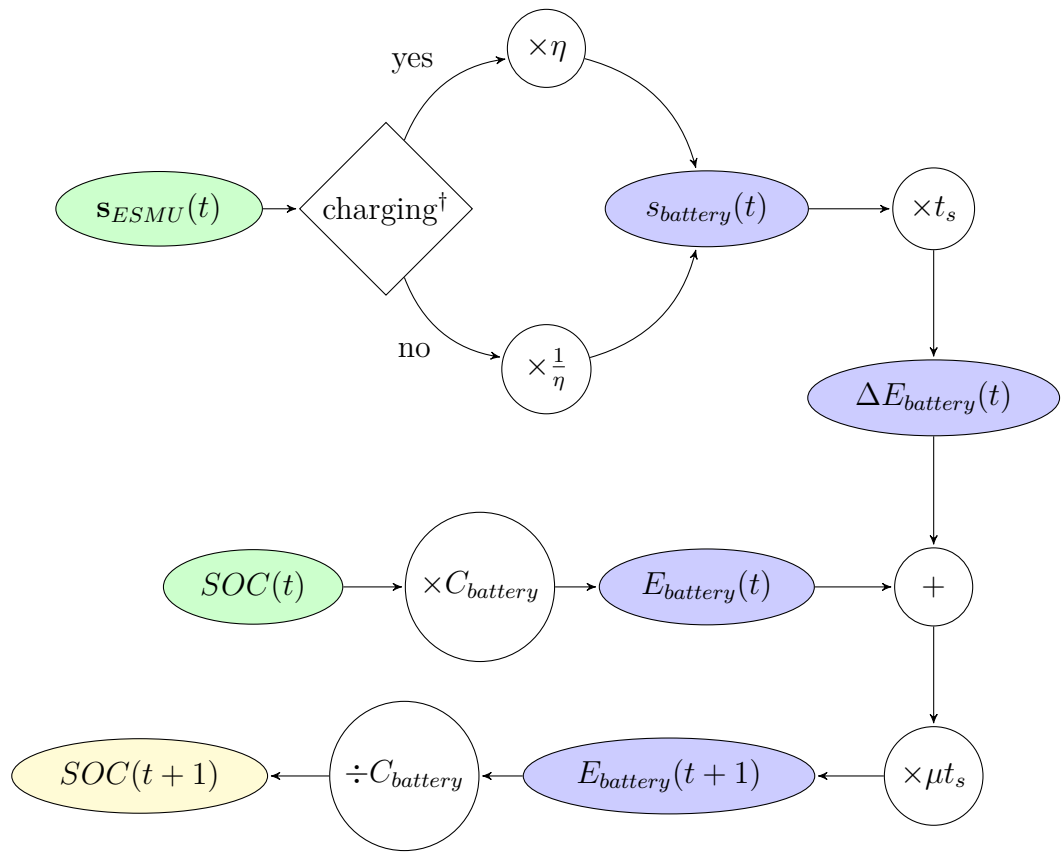


Figure 3.10: Flowchart to calculate the next SOC (i.e. $SOC(t+1)$) based on current ESMU power (i.e. $s_{ESMU}(t)$) and current SOC (i.e. $SOC(t)$)

3.4 Closed-Loop Optimisation Method

In the previous two sections, the key network parameters and associated cost functions have been established. Then the used network models, data and battery models were explained. Now, the implemented method on generating a traditional ESMU schedules is presented, before presenting the novel approach of adjusting this schedule using on-line readings.

3.4.1 ESMU Schedule Generation

As discussed in the literature review in Chapter 2, the main goals when scheduling battery operation are to achieve “valley-filling” and “peak-shaving” behaviour. It has been identified, that both the Peak-to-Average Ratio (PAR) as well as the min-max-difference (MMD) are good indicators of how well the pursued behaviours have been implemented. Therefore, a half-hourly PAR scheduling cost, $\zeta_{PAR}^*(\mathbf{s}_{ESMU}^*, \mathbf{s}_{network\ load}^*)$, and a half-hourly MMD scheduling cost, $\zeta_{MMD}^*(\mathbf{s}_{ESMU}^*, \mathbf{s}_{network\ load}^*)$, are defined as follows:

$$\zeta_{PAR}^*(\mathbf{s}_A^*, \mathbf{s}_B^*) := \frac{\max_t |\mathbf{s}_A^*(t) + \mathbf{s}_B^*(t)|}{\frac{1}{T^*} \sum_{t=1}^{T^*} [\mathbf{s}_A^*(t) + \mathbf{s}_B^*(t)]} \quad (3.22)$$

where $\mathbf{s}_A^*(t) \in \mathbf{s}_A^*$ and $\mathbf{s}_B^*(t) \in \mathbf{s}_B^* - 1$

$$\zeta_{MMD}^*(\mathbf{s}_A^*(t), \mathbf{s}_B^*(t)) := \frac{\max_t (\mathbf{s}_A^*(t) + \mathbf{s}_B^*(t)) - \min_t (\mathbf{s}_A^*(t) + \mathbf{s}_B^*(t))}{\frac{1}{T^*} \sum_{t=1}^{T^*} [\mathbf{s}_A^*(t) + \mathbf{s}_B^*(t)]} \quad (3.23)$$

where $\mathbf{s}_A^*(t) \in \mathbf{s}_A^*$ and $\mathbf{s}_B^*(t) \in \mathbf{s}_B^*$

Both costs are functions of the entire half-hourly ESMU schedule, \mathbf{s}_{ESMU}^* , and the entire half-hourly network load profile, $\mathbf{s}_{network\ load}^*$, where only the ESMU schedule is adjustable by an optimisation algorithm. For this piece of work, a Sequential

Quadratic Programming (SQP) approach was chosen to solve the following minimisation problem. Reasons behind this choice are the SQP's robustness and speed, since it is built on the well established Newton-Raphson Method, as well as its ability to cope with nonlinear constraints. It is this latter point that is most important, since the battery model's solving constraints are inherently nonlinear; the Newton-Raphson Method by itself is unable to solve with this kind of nonlinear constraints. The final minimisation problem that was passed into the SQP solver can be formulated as:

$$\begin{aligned} \min_{\mathbf{s}_{ESMU}^*} & \zeta_{PAR}^*(\mathbf{s}_{ESMU}^*, \mathbf{s}_{network\ load}^*) + \zeta_{MMD}^*(\mathbf{s}_{ESMU}^*, \mathbf{s}_{network\ load}^*) \\ \text{s.t. } & \left\{ \begin{array}{l} s_{battery}(t) \leq C_{factor} \times C_{battery} \forall t \\ |s_{ESMU,p}(t)| \leq S_{rating} \forall p \forall t \\ 0 \leq SOC(t) \leq 1 \forall t \end{array} \right. \end{aligned} \quad (3.24)$$

To summarise, this operation therefore minimises two costs by adjusting the half-hourly ESMU schedule, \mathbf{s}_{ESMU}^* , given a certain constant half-hourly network load (or forecast) $\mathbf{s}_{network\ load}^*$. These two costs both capture the PAR and MMD of the resulting power profile, and when minimised to zero, indicate a perfectly flat power curve. The minimisation is constrained to not exceed the battery's maximum charge/discharge rate (i.e. $s_{battery}(t) \leq C_{factor} \times C_{battery} \forall t$), to not exceed the PMU's phase power rating (i.e. $|s_{ESMU,p}(t)| \leq S_{rating} \forall p \forall t$), and to not over- or under-charge the battery (i.e. $0 \leq SOC(t) \leq 1 \forall t$).

For the work presented in this chapter, the supplied half-hourly network load (or forecast) was extrapolated from sub-half-hourly data. This forecast can be seen as if it had been generated with perfect foresight. Treating it in such a way does not further skew the already imperfect performance that is obtained when applying the resulting half-hourly schedule. Therefore, any additional improvement or worsening

is the result of the sub-half-hourly schedule adjustments. In the following figure, a visualisation is provided where the impact of this half-hourly ESMU schedule becomes apparent.

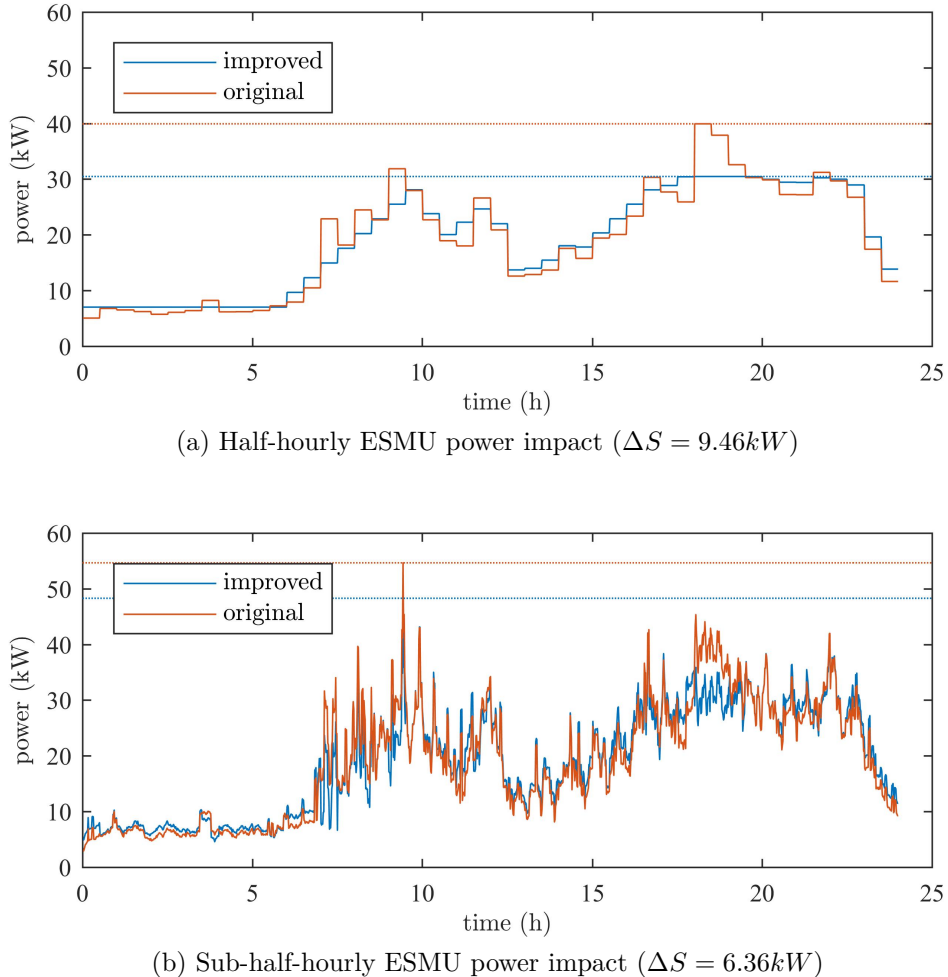


Figure 3.11: Impact of half-hourly ESMU schedule on sub-half-hourly power profile

Figure 3.11 shows the original half-hourly network load and the improved network when adding the half-hourly ESMU schedule. For this preliminary result, no network simulations have been carried out, as it should show an idea ESMU impact on the network's load. This positive impact can be seen, since the half-hourly profile in Figure 3.11a is dominated by an evening peak in demand. However, the actual sub-half-hourly demand, as it is plotted in Figure 3.11b, has a much larger demand spike during the morning hours, which is not addressed as strongly as the evening peak.

Therefore, the compared peak power shaving dropped from 9.46kW to only 6.36kW, although only 50% of the battery’s discharge capacity is used. Nonetheless, the overall improvement yielded by the ESMU schedule is still noticeable (given that it was scheduled using perfect half-hourly foresight).

In the following section, the underlying closed-loop schedule adjustment method is explained, where it will be shown how individual key network parameters can be positively impacted without deviating from this already optimised half-hourly schedule. The constraint of having to follow this half-hourly ESMU schedule is lifted in Chapter 4, where a real-time schedule adjustment method is proposed and researched.

3.4.2 Closed-Loop Schedule Adjustment

To quickly summarise, the following key network parameters are used in this chapter:

- substation phase voltages, $v_{ss,p}(t) \in \mathbf{v}_{ss}(t)$,
- ESMU phase voltages, $v_{ESMU,p}(t) \in \mathbf{v}_{ESMU}(t)$,
- all load voltages, $v_{load,i}(t) \in \mathbf{v}_{load}(t)$,
- substation apparent phase power, $s_{ss,p}(t) \in \mathbf{s}_{ss}(t)$,
- substation phase currents, $i_{ss,p}(t) \in \mathbf{i}_{ss}(t)$,
- all line currents, $i_{line,l,p}(t) \in \mathbf{i}_{line}(t)$, and
- all network losses, $s_{losses}(t)$.

Together with these key network parameters, and the cost functions defined in Section 3.2, a weighted sum of all costs is generated and formalised into the following global cost function:

$$\begin{aligned}
\zeta(v_{ss,p}(t), v_{ESMU,p}(t), \mathbf{v}_{load}(t), \mathbf{s}_{ss}(t), \mathbf{i}_{ss}(t), \mathbf{i}_{line}(t), s_{losses}(t), \boldsymbol{\alpha}) := \\
\alpha_1 \zeta_{\text{voltage}}(v_{ss,p}(t)) + \alpha_2 \zeta_{\text{voltage}}(v_{ESMU,p}(t)) + \alpha_3 \zeta_{\text{load voltage}}(\mathbf{v}_{load}(t)) \\
+ \alpha_4 \zeta_{\text{unbalance}}(\mathbf{s}_{ss}(t)) + \alpha_5 \zeta_{\text{PF}}(\mathbf{s}_{ss}(t)) + \alpha_6 \zeta_{\text{neutral load}}(\mathbf{s}_{ss}(t)) \\
+ \alpha_7 \zeta_{\text{fuse utilisation}}(\mathbf{i}_{ss}(t)) + \alpha_8 \zeta_{\text{line utilisation}}(\mathbf{i}_{line}(t)) + \alpha_9 \zeta_{\text{losses}}(s_{losses}(t)) \forall t
\end{aligned}$$

where $p \in [1, \dots, P]$ and $P \in \mathbb{N}$ and $\alpha_n \in \boldsymbol{\alpha}$ (3.25)

Here, $\boldsymbol{\alpha}$ is a binary choice vector, with which the weight of the global cost function can easily be adjusted. In other words, this vector allows to target the network improvement based by focusing on a specific cost, rather than optimising the network operation based on the complete set of (sometimes contradicting) costs. Since all key network parameters are outputs of the power flow simulations and not directly adjustable, and for simpler notations throughout this section, the global cost function is shortened to $\zeta(\boldsymbol{\alpha})$.

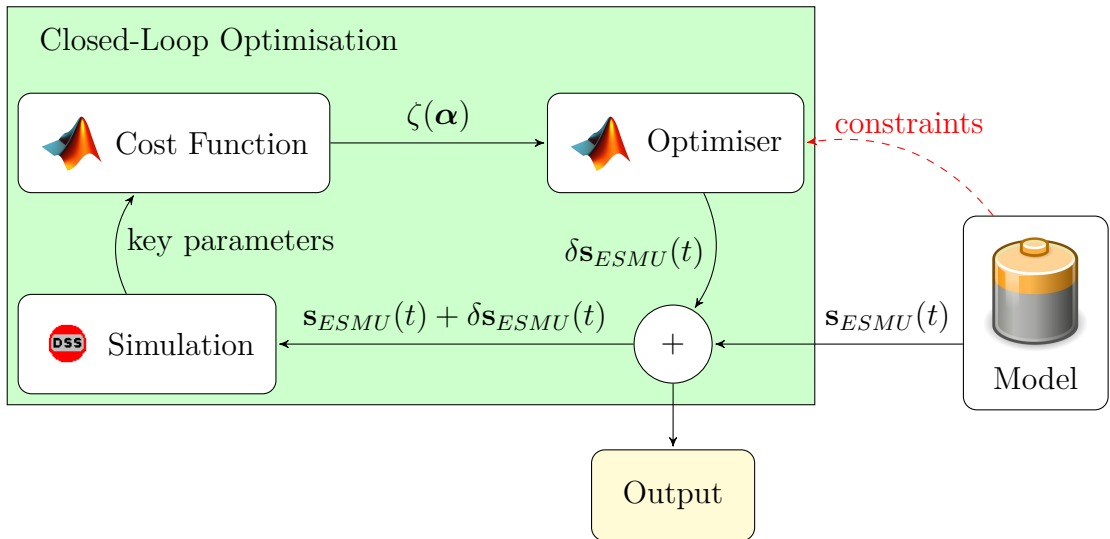


Figure 3.12: ESMU schedule adjustment flow diagram

The underlying method that performs the proposed closed-loop optimisation is captured in the next Figure 3.12. Here, for each time slot, t , a pre-scheduled ESMU

power vector, $\mathbf{s}_{ESMU}(t)$, is extracted and adjusted by an offset vector, $\delta\mathbf{s}_{ESMU}(t)$. This offset vector is found through the aforementioned optimiser that minimises the global cost function, $\zeta(\boldsymbol{\alpha})$, by repetitively running power flow simulations of the IEEE distribution feeder. Once the adjusted ESMU schedule (i.e. $\mathbf{s}_{ESMU}(t) + \delta\mathbf{s}_{ESMU}(t)$) is no longer changed by the optimiser, the closed-loop optimisation process ends and the simulation continues to the next time slot (i.e. $t + 1$).

Since $\delta\mathbf{s}_{ESMU}(t)$ must not impact the underlying half-hourly ESMU schedule, one more constraint is defined. This constraint assures that the sum of all phase powers in the adjustment vector equates to zero, hence keeping the internal battery's dis/charging power the same. Including the previously mentioned battery system constraints, which ensure that the ESMU operates within its technical limitations (e.g. to not over- or undercharge the battery), the minimisation problem for the closed-loop optimisation mechanism can be formulated as follows:

$$\min_{\delta\mathbf{s}_{ESMU}(t)} \zeta(\boldsymbol{\alpha}) \text{ s.t. } \begin{cases} \sum_{p=1}^P \operatorname{Re}(\delta s_{ESMU,p}(t)) = 0 \forall t \\ s_{battery}(t) \leq C_{factor} \times C_{battery} \forall t \\ |s_{ESMU,p}(t)| \leq S_{rating} \forall p \forall t \\ 0 \leq SOC(t) \leq 1 \forall t \end{cases} \quad (3.26)$$

where $\delta s_{ESMU,p}(t) \in \mathbf{s}_{ESMU}(t)$ and $P \in \mathbb{N}$

3.4.3 Method Execution and Result Assessment Procedure

After having established what parameters to focus on when trying to improve network operation, and after having established how the closed-loop optimising method aims to achieve this improvement, the performance assessment for the improvement method is introduced now. To support the explanation of the evaluation procedure, the entire assessment procedure is captured in Figure 3.13.

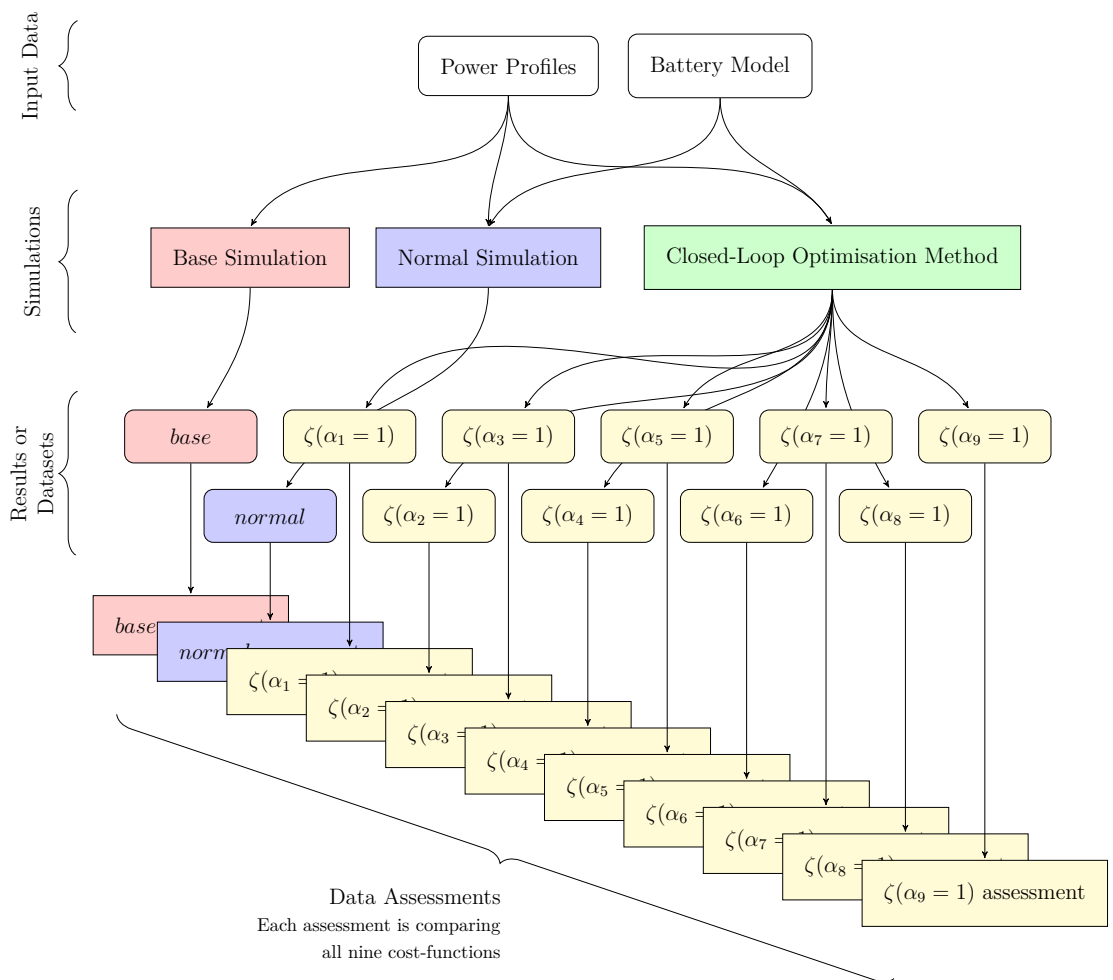


Figure 3.13: Method execution and results assessment flowchart

All in all, there are eleven datasets of simulation results to be assessed and compared. These results are obtained from a *base* simulation, a *normal* simulation and nine additional simulations where individual cost-functions were minimised. More specifically, the *base* case is the outcome of running an entire day of power profiles without any ESMU intervention. This case represents the baseline or network performance which should be improved by any ESMU intervention. The **normal** case captures the simplest of all ESMU interventions, since for this case, the ESMU executes its normal half-hourly schedule without any additional schedule modification. Comparing the *base* and *normal* cases does show the direct impact of the ESMU on the network's operation. As mentioned above, the remaining nine datasets are results of nine different cases where the ESMU schedule is adjusted on a sub-half-hourly level. The adjustment for each case is designed to minimise one underlying cost-function, whilst conforming to the ESMU's overall half-hourly charging and discharging profile. In order to treat each cost-function separately α is set to focus on each cost independently, e.g. by setting $\alpha_1 = 1$ and $\alpha_2 = \alpha_3 = \dots = \alpha_9 = 0$. For simplicity, the flowchart in Figure 3.13 abbreviates the specific costs by only indicating which entry in the α vector is set to 1, e.g. $\zeta(\alpha_1 = 1)$ for the preceding example.

All eleven datasets are then assessed in the same manner in order to compare the impact they had had on the network performance. This underlying assessment is broken into three parts for each dataset:

1. **Time Series Analysis** - The underlying raw profiles are plotted and compared against their respective counterpart cases, in order to link the immediate network impacts to their physical meaning. For the same profiles, their corresponding cost profiles are calculated plotted. This is done to highlight how the profiles are interpreted by the cost-functions in terms of improvement (i.e. lower cost) or worsening (i.e. increased cost).
2. **Difference Analysis** - The difference in cost profiles, compared to the respec-

tive *base* or *normal* case, is calculated and boxplots of these differences are presented to show a statistical spread of improvements or worsening. For these plots, a generally positive boxplot skew indicates a general improvement of the underlying network parameters, whilst a generally negative skew does indicate worse performance in regards to the underlying network parameters.

3. Probability Density Analysis - A set of Probability Density Functions (PDF) is derived for each cost profile using the well established kernel density estimation. These PDFs indicate the probability that a certain cost value occurs. An improvement is noted when the PDF is shifted towards the lower cost values, whereas a shift towards higher cost values worsened the network performance.

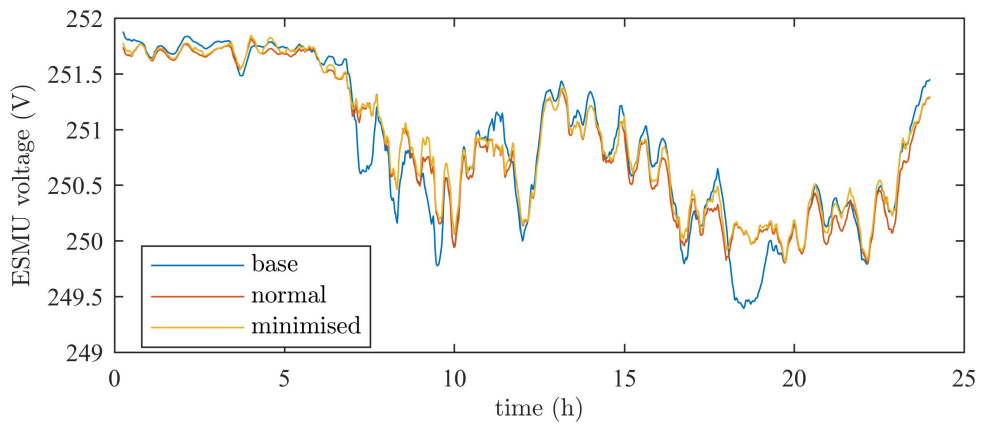
3.5 Results and Discussion

In this section, all results from the three assessment parts that were outlined in Section 3.4.3 are presented, and they are briefly discussed, too. Each assessment focus on improvements in voltage level, improvements in network efficiency (i.e. power quality and network losses), and improvements in resource utilisation, in that order. For completeness and transparency however, the complete analysis of the entire data for each part of the assessment is included in this Thesis' Appendix, Section A.1.

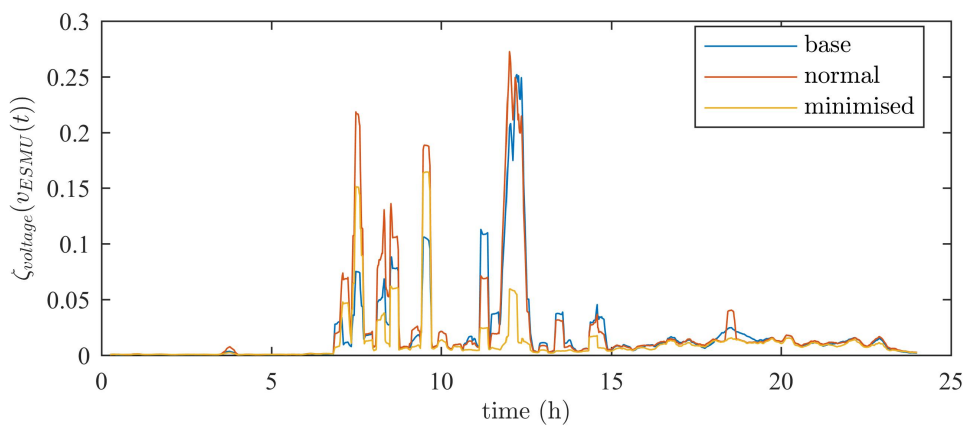
3.5.1 Time Series Analysis

The most direct impact on the network's voltage levels would be noticed at the ESMU's PCC. Therefore, any adjustments to the ESMU's schedule should be most noticeable, too, and its impact can clearly be observed in the figure below.

Here, in Figure 3.14a, the base and normal case's voltage profiles are plotted alongside the case for which the deviation from substation voltage is minimised. For reference, the nominal substation voltage (i.e. the default IEEE Test Case P2N volt-



(a) Voltage levels at ESMU's PCC when minimising its voltage deviation (nominal substation voltage included for reference)



(b) Cost associated with the minimisation of the ESMU's PCC voltage deviation

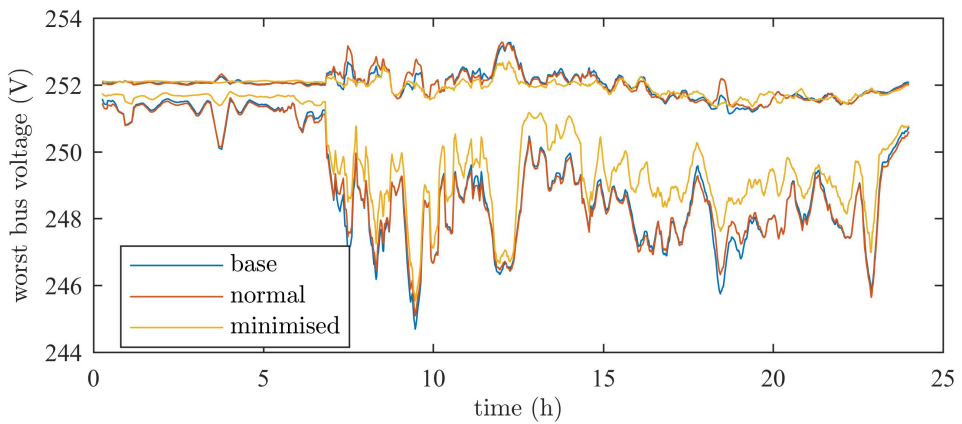
Figure 3.14: Voltage level modifications as noted at the ESMU's PCC by adjusting its schedule

age) has been included for reference. From this figure it can be observed that during the night's light load (i.e. from 0:00 to 6:00), the ESMU was capable of boosting its voltage towards its nominal feeder voltage. This is also the case during the lighter afternoon load (i.e. between 12:00-14:00). Yet during the rest of the day, the ESMU noticeably failed to match its PCC voltage to the network's nominal substation voltage. The reason behind this behaviour is the fact that the ESMU already reserved its resources to cater for its underlying half-hourly schedule. Therefore, the remaining resources to provide voltage support become more limited. Combined with the fact that the LV distribution network is more resistive than inductive (i.e. unlike HV transmission networks), reactive power injection to support voltage levels has a reduced impact. Nonetheless, due to the constant yet small availability of power resources, the ESMU was able to boost voltages by to some extent at all times; this can be seen in Figure 3.14b, where the associated cost has always been reduced in comparison to the base and normal.

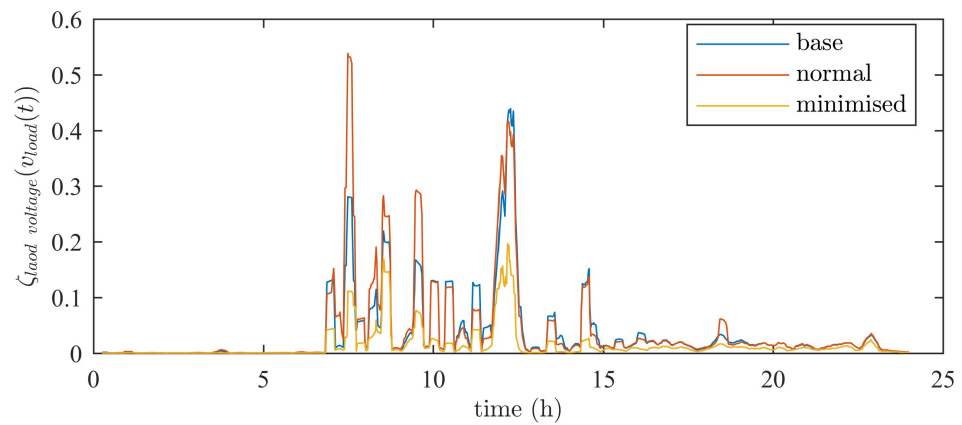
The ability to support voltage levels at the ESMU's PCC is interesting, yet to support voltage levels at all buses throughout the network is more relevant, since some of these buses are linked to customers, for which maintaining a constant voltage level is essential. Therefore, the next voltage plot inspects both the highest and lowest voltage level that was recorded throughout the network.

In Figure 3.15a, despite no voltage violations taking place due to the already boosted substation voltage, the ESMU's positive impact can be observed. Here, the difference between highest and lowest voltage in the network was noticeably reduced at all times and their average was brought closer to the network's nominal voltage. The ESMU's function to support the network in providing more stable voltage levels at customer endpoints can therefore be fulfilled. This fact is also reflected in the associated cost plot, i.e. in Figure 3.15b.

Beside providing stable voltage levels, power quality should also be upheld to



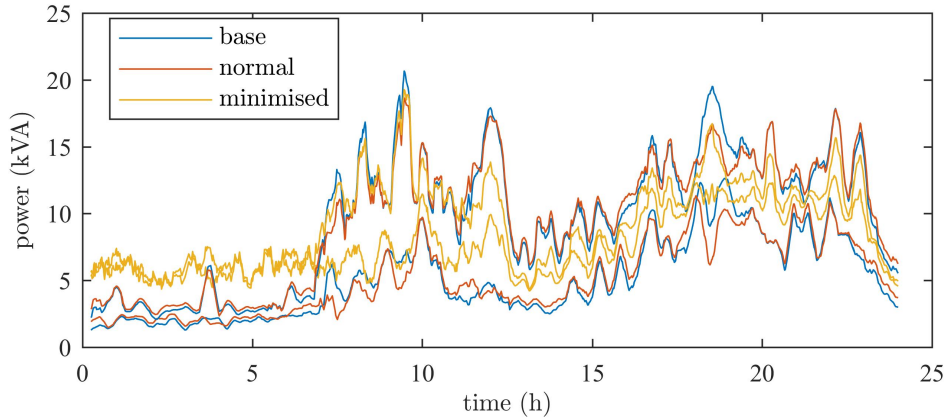
(a) Highest and lowest voltage levels that were recorded throughout the network when minimising the worst voltage deviation (nominal substation voltage included for reference)



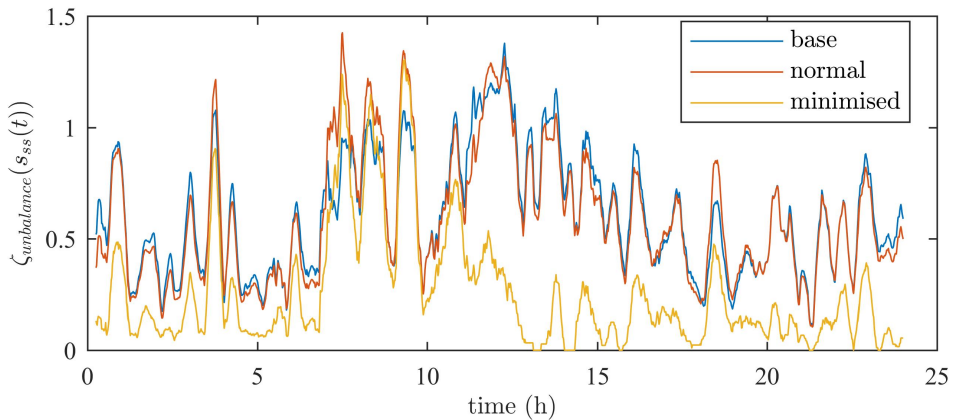
(b) Cost associated with the worst voltage deviation throughout the entire network

Figure 3.15: Voltage level improvements at all buses in the entire distribution network due to the ESMU schedule adjustment.

assure that the distribution network operates as efficient as possible. The first power related parameter that to indicate network efficiency is the phase unbalance.



(a) Network's highest and lowest phase power demand when phase unbalance was minimised



(b) Cost associated with the network's phase unbalance

Figure 3.16: Reduction of the network's phase unbalance due to the adjustment of the ESMU schedule.

In Figure 3.16a, the most and least loaded phases' power values are plotted against time. At all times, the sub-half-hourly adjustments of the ESMU's schedule could reduce the underlying phase imbalance. It did so by alleviate some load from the most loaded phase and utilise the unused capacity on the lighter loaded phases. Correspondingly, the associated phase unbalance cost has noticeably lowered in comparison to the normal and base cases. It should however be noted, that phase balancing behaviour during the morning hours is predominantly comprised of reactive power in-

jection and absorption, since the ESMU's half-hourly. Therefore, the tradeoff between adding additional strain on the network, versus balancing phases has to be taken into account. One unnecessary strain on the network is additional neutral power flow, which is inadvertently linked to phase unbalance.

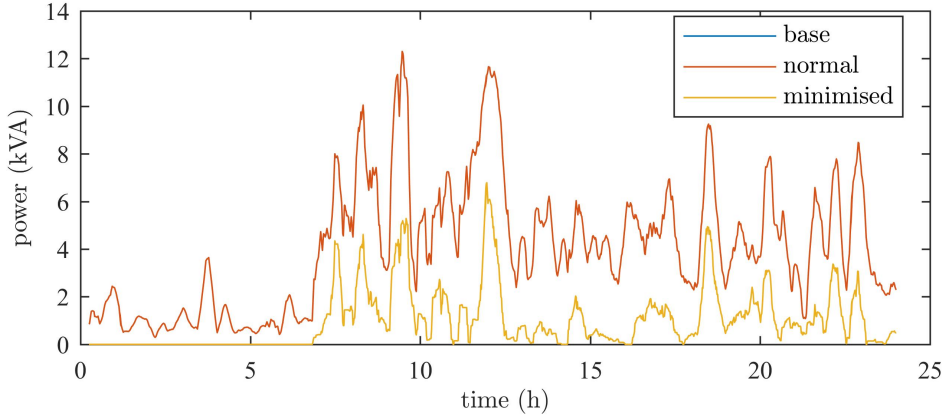


Figure 3.17: Neutral power reduction due to the ESMU schedule adjustments

The results plotted in Figure 3.17 show the network impact when adjusting the ESMU's schedule in order to minimise neutral power flow. Incidentally, when applying the normal half-hourly ESMU schedule, neutral power is not affected at all. The reason behind this was the choice of evenly assigning the scheduled power to all three phases, instead of taking into account the phases' loadings. Power factor on the other hand was impacted just by introducing the half-hourly ESMU schedule, as shown in the following figure.

Here, in Figure 3.18, the power factor cost is successfully reduced during the entire day, in comparison to the normal cases. In contrast, the base case had a constant power factor cost, due to aforementioned assignment of a constant power factor of 0.95 to all loads. In reality, however, any network's power factor varies over time since the number of inductive machines and their associated inductive load varies constantly. Nonetheless, the results would be similar but more variable when applied to a network with varying power factor, since the aim when adjusting the ESMU

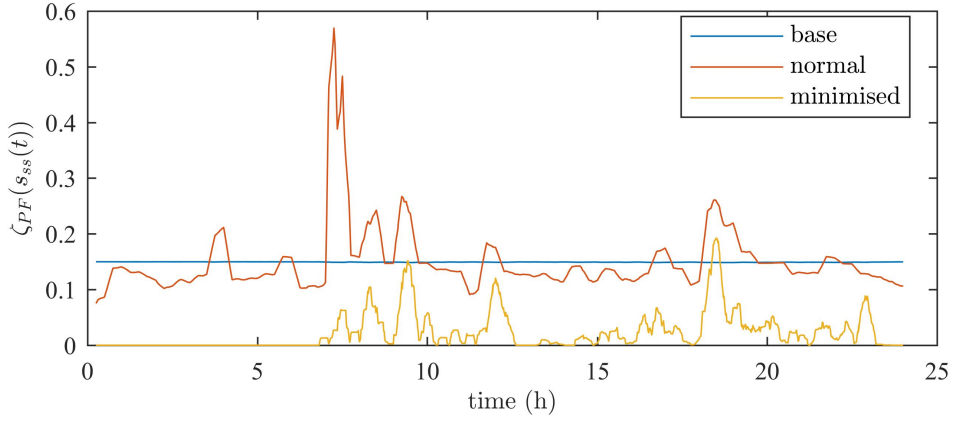


Figure 3.18: Power factor cost improvements due to the adjustment of the ESMU schedule

schedule was to reduce the power factor's deviation from unit power factor. The final parameter that indicates system efficiency are the distribution losses.

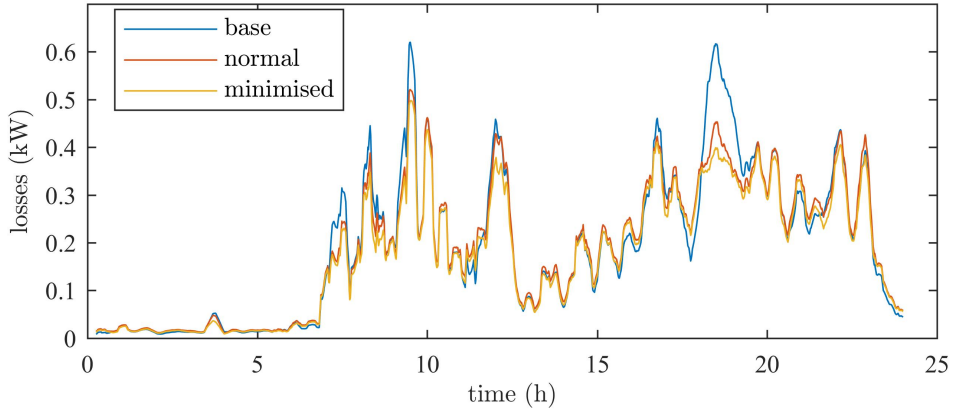


Figure 3.19: Instantaneous losses of the distribution network when adjusting the ESMU schedule in order to reduce the former (energy lost: 75.9Wh for base; 74.7Wh for normal; 69.9Wh for minimised).

Figure 3.19 shows the reduction in distribution losses that were achieved when adjusting the ESMU schedule accordingly. Again, the schedule adjustment reduced losses throughout the entire day. In fact, an additional 6.42% of energy savings could be achieved, simply by adjusting the ESMU's power injection and absorption behaviour. Whilst this amount of energy may seem insignificant on a small scale, saving this amount of energy on a national level could potentially benefit the entire

power network. However, losses are difficult to measure and attempting to do so would most likely outweigh the benefits.

Instead, a better way of relieving stress from the power network is to minimise its assets utilisation by mitigating demand spikes. Since the ESMU was constraint not to deviate from its underlying half-hourly schedule, only phase related demand differences could be addressed. Those differences could however be addressed successfully, as shown in the following figure.

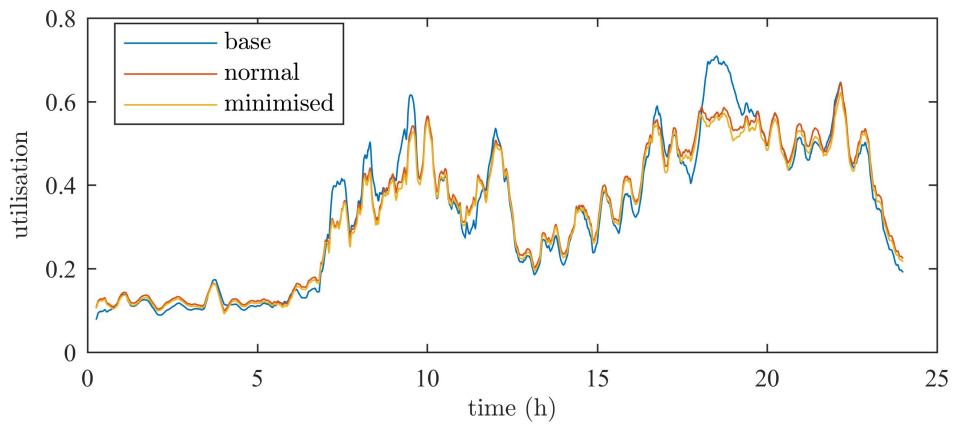


Figure 3.20: Improvement of the worst line utilisation across the entire network when adjusting the ESMU schedule correspondingly.

Whilst the worst line utilisation is predominantly driven by the half-hourly charging and discharging behaviour of the ESMU, a subtle reduction could be achieved throughout the entire day, as shown in Figure 3.20. Yet as mentioned before, the constraint that is imposed due to the underlying half-hourly schedule significantly limits this improvement in network performance.

3.5.2 Difference Analysis

In order to gage the whether there is a statistical difference in network performance, a box-plot was generated for each case. The underlying data for each box-plot is the paired difference between the corresponding case's costs and the associated normal case's costs, i.e. when letting the ESMU operate normally, without adjusting its

schedule. Any positive difference in those costs indicates an improvement to the system's performance, whilst a negative difference would imply a worsening.

Here, the improvements for each individual cost are compared and plotted in Figure 3.21. A further set of comparing figures is also included in Appendix Section A.1.2, where the impacts on all costs, when minimising a for only an individual cost are compared. Instead of including all these figures in the main body of this Thesis, the sum of all costs is computed and included in a table to give a more comprehensive indication of these so called cross-cost improvements.

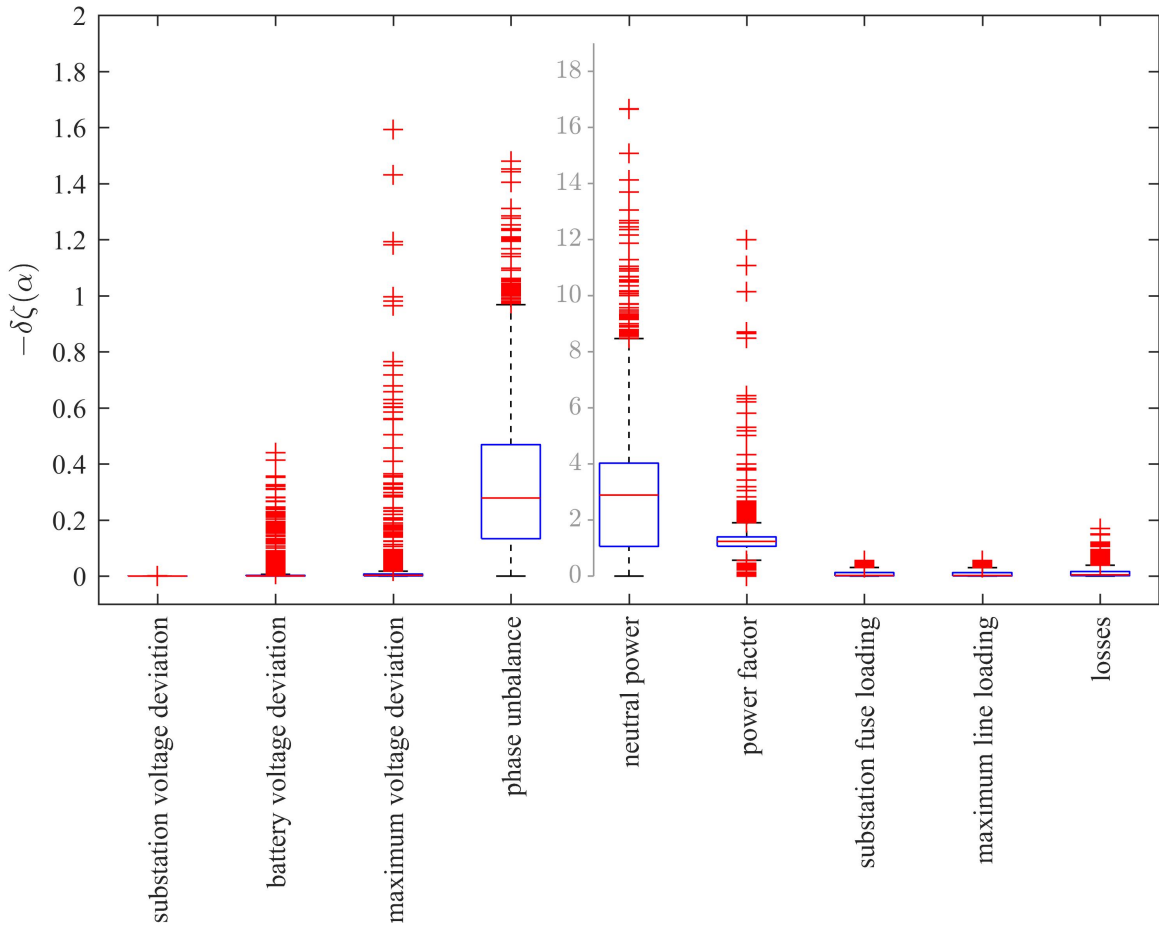


Figure 3.21: Cost-function improvement spread, when comparing against the normal ESMU operation case and when optimising for the underlying cost (a separate y-axis is introduced for the optimisation of “neutral power”).

In Figure 3.21, it can be seen that the most significant cost related impact on the network was on the improvement of phase unbalance, neutral power and power factor.

The reason for this noticeably larger impact is that the ESMU can assign its scheduled active power in an arbitrary manner to all three phases, as long as the predetermined half-hourly schedule is followed. It is this constraint of having to obey the schedule, that limits the impact on all other key network parameters. Reactive power on the other hand is not directly limited to this constraint, since it is not scheduled as such. The only limit that applies to the ESMU’s reactive power injection capabilities, is the remaining PMU capacities when applying the active powers in order to follow the half-hourly schedule. Also, unlike active power, reactive power has a smaller impact on the LV network due to its physical property, i.e. being more resistive than inductive. Nonetheless, all key network parameters were impacted positively when they became subject to their associated cost-function minimisation.

To summarise the aforementioned cross-cost improvements (which are presented in detail in the Appendix, Section A.1.2), all costs are calculated for all minimisation cases, compared against the normal case, and accumulated into a single value. This value is defined as the “cumulative cost difference”. Additionally, the normal case is compared to the base case in a similar manner. This was done since it is interesting to see how the half-hourly schedule impacted the network.

The cumulative cost differences are tabulated in Table 3.1. Every improvement in system operation is reflected as a reduction in cost, when compared to the corresponding normal or base case. Therefore, a positive cumulative cost difference indicates, that over an entire day, the system operation improved in regards to the given cost. Here, these improvements, i.e. positive cumulative cost differences, have been highlighted.

As expected, all entries along the diagonal, i.e. where the evaluated cost is also the cost that was minimised for the underlying case, nearly always show the largest cumulative cost differences. It is also interesting to see, how a specific cost minimisation had noticeable impacts on different cumulative cost measures. For example,

	minimisation cases					
	normal					
substation voltage deviation	0.00	0.08	-2.49	-1.39	-4.89	-8.72
battery voltage deviation	-5.01	-0.40	15.52	17.04	9.14	14.93
maximum voltage deviation	-6.83	-1.15	28.22	36.42	24.66	33.05
phase unbalance	12.15	40.93	284.87	380.57	490.22	351.35
neutral power	-0.83	-96.72	2303.70	1642.37	2698.78	4415.85
neutral power	-0.27	159.42	-7.63	-37.25	-633.30	-314.11
power factor	5.14	13.34	-0.43	-8.69	-51.76	-72.68
substation fuse loading	4.53	12.88	-6.17	-10.04	-80.41	-97.30
maximum line loading	4.34	7.22	13.38	-4.46	-46.37	-66.32
losses						
maximum line loading						
substation fuse loading						
neutral power						
phase unbalance						
maximum voltage deviation						
battery voltage deviation						
substation voltage deviation						
losses						

Table 3.1: Cross-cost improvements due to adjustments to the original ESMU schedule.

adjusting the ESMU schedule to achieve the largest reduction in distribution losses (i.e. far right column) had an impact on all key network parameters. This impact was also positive in nature for all key network parameters (apart from substation voltage deviation).

Then again, although the network optimisation for an optimised line and fuse loading did result in a positive cumulative cost difference, reduction in power factor had a more significant positive impact. The reason behind this is that instantaneous apparent power contributes to the loading. This means, that increasing the power factor inadvertently reduces reactive load, which in turn lowers the total current flowing into the system. Not knowing what cost to address first, makes it difficult for the used solving algorithm to find the global minimum. To improve the performance of the adjusted ESMU schedule, one could concatenate the cost minimisation in series to locate regions where lower minima may be found. In this case at least, maximising the network's power factor before addressing fuse and line utilisation would have been a better choice.

3.5.3 Probability Density Analysis

The final part of analysing the results is to statistically determine, whether the cumulative cost differences are significantly different. To do so, the probability density functions (PDF) of the cost differences

3.6 Summary

In this chapter, a method to adjust an ESMU schedule to support network operation has been developed and tested. The underlying schedule was a half-hourly dis/charge profile that the battery had to follow. Through the adjustment of the three-phase ESMU power, both active and reactive power could be adjusted in order to min-

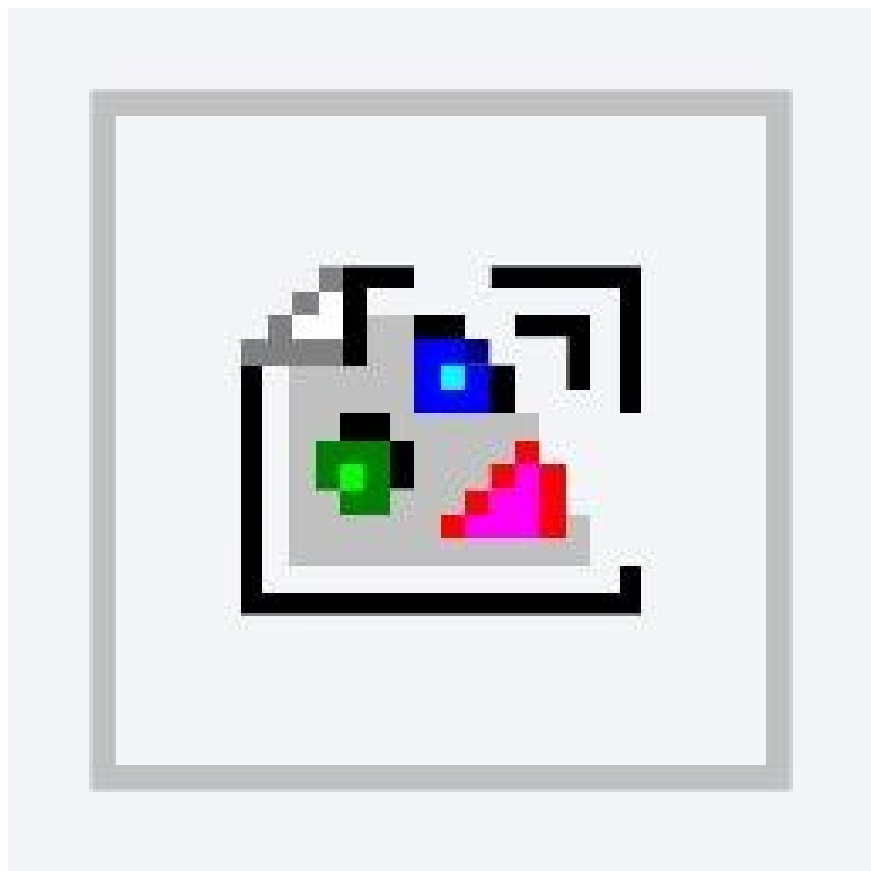


Figure 3.22: p -values for null hypothesis test

imise a set of defined costs. The results indicate, that when explicitly focusing on the improvement of certain key network parameters, then in every case the derived cost reduced. Furthermore, for most cost minimisation attempts, different costs were impacted, too (i.e. loss minimisation impacted nearly all other costs). Using cumulative cost differences it was shown that a net cost reduction could be achieved, when implementing the proposed schedule adjustment method. This fact is also the reason why the resulting probability density analysis, using the two-paired *t*-test and Kolmogorov-Smirnov test, disproved the null hypothesis as it was formulated for this chapter. Therefore, there is strong evidence that adjustments of ESMU schedules on a sub-half-hourly bases have positive impacts on the distribution network's operation.

The main limitation of the proposed method is however the battery's half-hourly schedule. It dictates the total active power that has to be injected into or absorbed from the distribution network. Also, this schedule inadvertently dictates the remaining overhead in reactive power that may be compensated for on each phase. Therefore, the next chapter addresses how the active power schedule may be corrected in real-time.

Chapter 4

Real-Time Adjustment of Battery Operation using MPC Guided Schedule Deviation

4.1 Overview

It has been established how the adjustment of an ESMU schedule at sub-half-hourly resolution, whilst keeping the battery’s dis/charge profile constant, does yield improved network operation. Adjusting apparent power on a phase by phase basis, where the summed active power offset is constrained to zero and the total apparent power is constrained to the ESMU’s power ratings, was proven to be a valid method for adjustment. Unlike traditional execution of static schedules, such methods provided more ESMU flexibility and allowed the device to respond to otherwise uncompensated variations in demand. But just like a traditional execution of a static schedule, such methods also constrain active power offset, resulting in highly predictable charging and discharging of the battery.

This fundamental constraint can be seen in previous research [20, 21], as well as

the work presented in Chapter 3 [24], and is set by a strict overlying half-hourly schedule that must not be violated. To achieve higher ESMU flexibility, two options exist:

1. remove the overlying half-hourly schedule and default to a set-point ESMU control, or
2. loosen the constraint and use the predetermined half-hourly schedule as a ESMU guidance instead of static control.

Many experts would agree that the former approach is easier to implement, since inexpensive feedback mechanisms may be used, yet it also removes control over the device, which could be disadvantageous for DNOs (or whoever aims to yield a profit from the ESMU operation). In other words, although the ESMU may operate using its internal control mechanisms, it cannot receive any external control signals, and therefore cannot be used for other energy dependent functions. These functions include DSR actions, arbitrage operation, or any other service for which a predetermined energy volume needs to be made available. If there is no schedule that assures this energy volume, then providing these aforementioned functions and exploiting their associated revenue streams is no longer an option; despite the ESMU being more flexible.

Therefore, in this chapter, the second option is pursued. A high-resolution closed-loop control system is developed that uses both a half-hourly schedule and a model based power forecast. The half-hourly schedule is interpolated into a sub-half-hourly set of instructions and, together with the model, forms a MPC. The MPC is used to predict the next future network power, therefore allowing the controller to compensate for otherwise unmitigated sub-half-hourly power peaks. To apply this MPC two on-line controllers based on Proportional Integral Derivative (PID) control are used. PID was chosen due to its simple controller structure that can be realised with

ease, and because PID can be tuned for guaranteed system stability, robustness and dynamic performance [25, 26, 27, 28]. Performance of this novel approach is measured by comparing the resulting power profiles with baseline power profiles. Also, to include the effect of erroneous schedules on the control system’s performance, realistic half-hourly forecasts are used instead of assuming perfect half-hourly foresight. The resulting data is analysed statistically and tested with the following null hypothesis:

Introducing minimalistic deviation from a ESMU schedule yields no significant improvement in network operation.

Here, the “*minimalistic deviation*” is defined in the next section, alongside the MPC models as well as the proposed dual PID controller layout. Also, the measure of “*improvement*” is explained. Then how the half-hourly and sub-half-hourly datasets and forecasts are obtained is explained. How they are used in different case studies is detailed in the method section, after which the results are presented and discussed. In the end, the key findings and null hypothesis rejection (where $p < 5\%$) are summarised.

4.2 MPC and PID Control Design

4.3 Data and Power Forecast Acquisition

4.4 Method and Case Studies

4.5 Results and Discussion

4.6 Summary

Chapter 5

Effects of Control Instruction Desynchronisation in a Distributed MAS of Smart-Charging Batteries

5.1 Overview

5.2 Summary

Chapter 6

Cooperative Operation of Distributed Batteries without Communications Infrastructure Needs

M. Zangs, P. Adams, et.al., “Distributed Energy Storage Control for Dynamic Load Impact Mitigation,” Energies, vol. 9, no. 8, p. 647, Aug. 2016

— Available: <http://dx.doi.org/10.3390/en9080647>

6.1 Overview

This chapter addresses the question how multiple batteries could be coordinated collectively...

6.2 Summary

Chapter 7

Conclusion

7.1 Overview of Main Findings

7.2 Knowledge Contribution

7.3 Research Limits

7.4 Future Work

Bibliography

- [1] National Grid, “Future Energy Scenarios 2016,” Tech. Rep. July, 2016.
- [2] National Grid, “Future Energy Scenarios 2015,” Tech. Rep. July, 2015.
- [3] T. D. de la Rubia, F. Klein, B. Shaffer, N. Kim, and G. Lovric, “Energy storage: Tracking the technologies that will transform the power sector,” tech. rep., Deloitte Development LLC., 2015.
- [4] D. Manz, R. Piwko, and N. Miller, “Look before you leap: The role of energy storage in the grid,” *IEEE Power Energy Mag.*, vol. 10, no. 4, pp. 75–84, 2012.
- [5] M. Kleinberg, N. S. Mirhosseini, F. Farzan, J. Hansell, A. Abrams, W. Katzenstein, J. Harrison, and M. A. Jafari, “Energy storage valuation under different storage forms and functions in transmission and distribution applications,” *Proc. IEEE*, vol. 102, no. 7, pp. 1073–1083, 2014.
- [6] Department for Business Enterprise and Regulatory (DBER) and Department for Transport (DfT), “Investigation into the Scope for the Transport Sector to Switch to Electric Vehicles and Plug- in Hybrid Vehicles,” tech. rep., 2008.
- [7] G. Strbac, C. K. Gan, M. Aunedi, V. Stanojevic, P. Djapic, J. Dejvise, P. Mancarella, A. Hawkes, D. Pudjianto, D. Openshaw, S. Burns, P. West, D. Brogden, A. Creighton, and A. Claxton, “Benefits of Advanced Smart Metering for De-

mand Response based Control of Distribution Networks,” Tech. Rep. April 2010, 2010.

- [8] F. R. Kalhammer, “Energy-Storage Systems,” *Sci. Am.*, vol. 241, no. 6, pp. 42–51, 1979.
- [9] J. Eyer and G. Corey, “Energy Storage for the Electricity Grid : Benefits and Market Potential Assessment Guide,” tech. rep., Sandia National Laboratories, 2010.
- [10] S. Rehman, L. M. Al-Hadhrami, and M. M. Alam, “Pumped hydro energy storage system: A technological review,” *Renew. Sustain. Energy Rev.*, vol. 44, pp. 586–598, 2015.
- [11] E. Barbour, “Energy Storage Sense,” 2015.
- [12] E. Barbour, I. A. G. Wilson, J. Radcliffe, Y. Ding, and Y. Li, “A review of pumped hydro energy storage development in significant international electricity markets,” *Renew. Sustain. Energy Rev.*, vol. 61, pp. 421–432, 2016.
- [13] The Economist, “Packing some power,” *Econ.*, 2012.
- [14] F. R. McLarnon and E. J. Cairns, “Energy Storage,” *Annu. Rev. Energy*, vol. 14, pp. 241–271, 1989.
- [15] H. Ibrahim, A. Ilinca, and J. Perron, “Energy storage systems-Characteristics and comparisons,” *Renew. Sustain. Energy Rev.*, vol. 12, no. 5, pp. 1221–1250, 2008.
- [16] H. Chen, T. N. Cong, W. Yang, C. Tan, Y. Li, and Y. Ding, “Progress in electrical energy storage system: A critical review,” *Prog. Nat. Sci.*, vol. 19, no. 3, pp. 291–312, 2009.

- [17] I. Hadjipaschalis, A. Poulikkas, and V. Efthimiou, “Overview of current and future energy storage technologies for electric power applications,” *Renew. Sustain. Energy Rev.*, vol. 13, no. 6-7, pp. 1513–1522, 2009.
- [18] X. Luo, J. Wang, M. Dooner, and J. Clarke, “Overview of current development in electrical energy storage technologies and the application potential in power system operation,” *Appl. Energy*, vol. 137, pp. 511–536, 2015.
- [19] W. Jewell and R. Ramakumar, “The effects of moving clouds on electric utilities with dispersed photovoltaic generation,” *IEEE Trans. Energy Convers.*, vol. EC-2, no. 4, pp. 570–576, 1987.
- [20] M. Rowe, T. Yunusov, S. Haben, C. Singleton, W. Holderbaum, and B. Potter, “A Peak Reduction Scheduling Algorithm for Storage Devices on the Low Voltage Network,” *IEEE Trans. Smart Grid*, vol. 5, no. 4, pp. 2115–2124, 2014.
- [21] T. Yunusov, W. Holderbaum, and B. Potter, “Cost function for sub-agent elements in multi-agent energy management system,” in *2011 2nd IEEE PES Int. Conf. Exhib. Innov. Smart Grid Technol.*, pp. 1–8, 2011.
- [22] American National Standards Institute Inc., “ANSI/NEMA MG 1-2011,” tech. rep., 2011.
- [23] Power and Energy Society, “Distribution Test Feeders,” 2017.
- [24] M. Zangs, T. Yunusov, W. Holderbaum, and B. Potter, “On-line adjustment of battery schedules for supporting LV distribution network operation,” *2016 Int. Energy Sustain. Conf. IESC 2016*, 2016.
- [25] I. Rasoanarivo and F. M. Sargas, “Multi-objective analysis for designing and controlling micro-grids under multi-control with PID, MHCC and FOPID controllers,” in *Conf. Rec. - IAS Annu. Meet. (IEEE Ind. Appl. Soc.)*, pp. 1–8, 2013.

- [26] C. Jianbo, C. Binggang, C. Wenzhi, and X. Peng, “Neural network self-adaptive PID control for driving and regenerative braking of electric vehicle,” in *Proc. IEEE Int. Conf. Autom. Logist. ICAL 2007*, pp. 2029–2034, 2007.
- [27] F. Betin, A. Sivert, B. Nahid, and G. A. Capolino, “Position control of an induction machine using variable structure control,” *IEEE Trans. Mechatronics*, vol. 11, no. 3, pp. 358–361, 2006.
- [28] A. Algaddafi, N. Brown, R. Gammon, S. A. Altuwayjiri, and M. Alghamdi, “Improving Off-Grid PV System Power Quality , and Comparing with Grid Power Quality,” in *2016 Int. Conf. Electron. Information, Commun.*, (Danang, Vietnam), pp. 1–6, 2016.

Appendix A

Additional Results

A.1 Improving operation performance of battery schedules at sub-half-hourly resolution

A.1.1 Additional Time Series Analysis

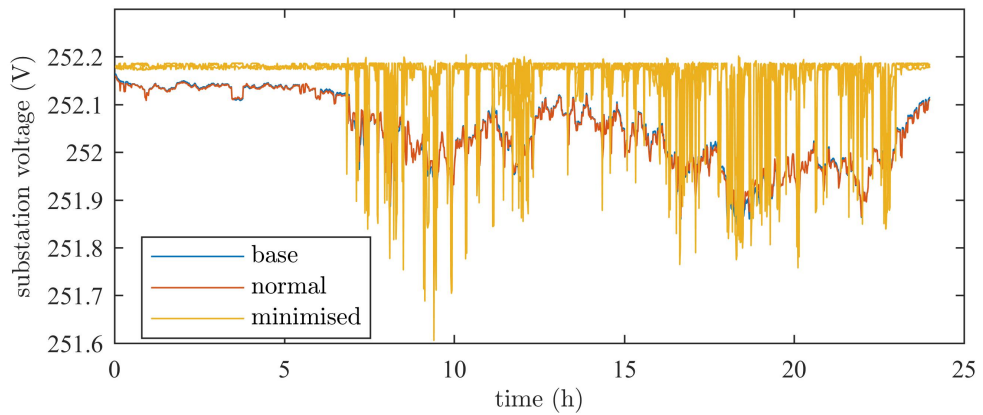
Since the plots in Section 3.5.1 are averages over a 10 minute moving average window (in order to aid visual representation of the volatile data), the raw and unfiltered data is included for reference in this appended section.

A.1.2 Additional Difference Analysis

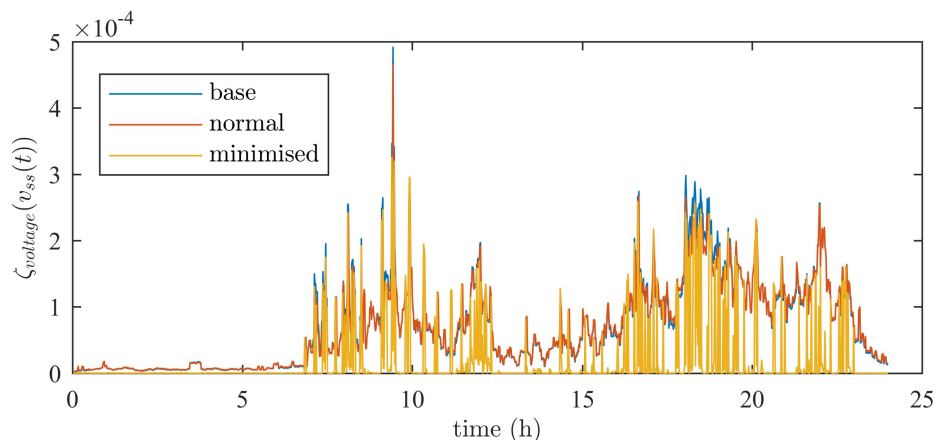
Only the cost differences for the case of actual cost minimisation were compared in Section 3.5.2. Therefore, all remaining cost differences have been included in this appended section.

A.1.3 Probability Density Analysis

The following plots are similar to those presented in 3.5.3 and have been included for completeness sake.



(a) Voltage levels as measured at the substation



(b) Cost associated with the voltage levels as measured at the substation

Figure A.1: Additional substation voltage level comparison between base, normal and the case where the ESMU's schedule was adjusted.

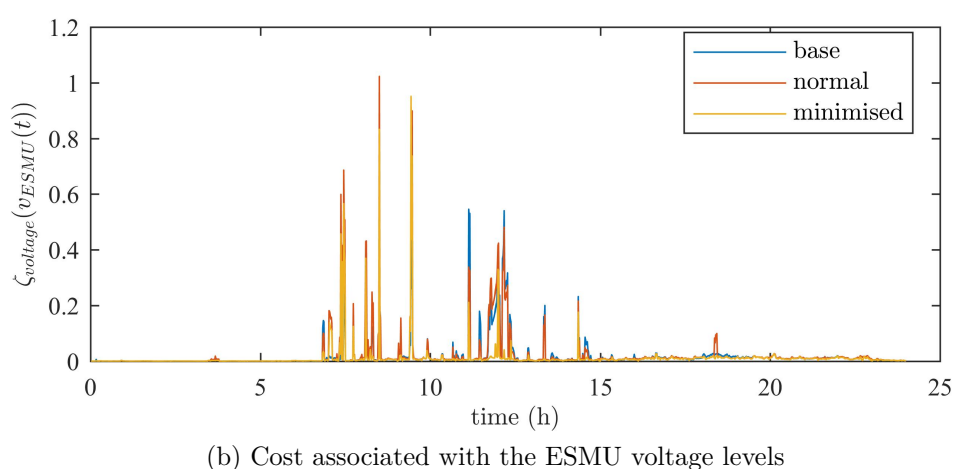
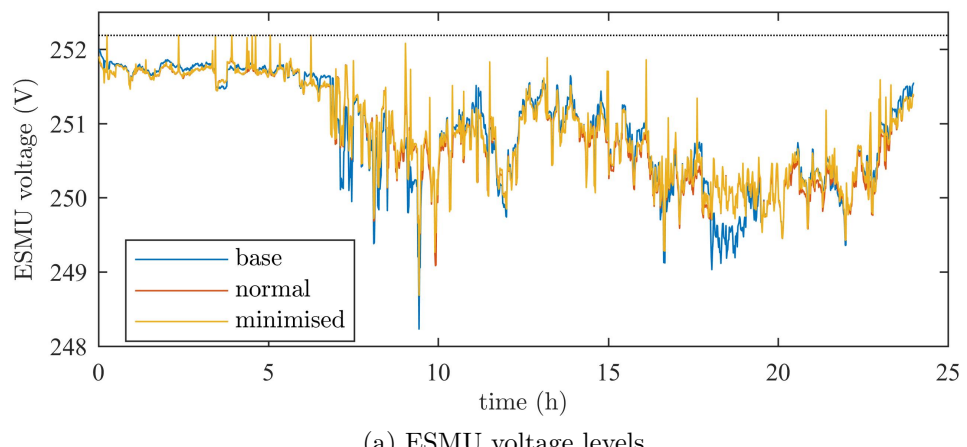
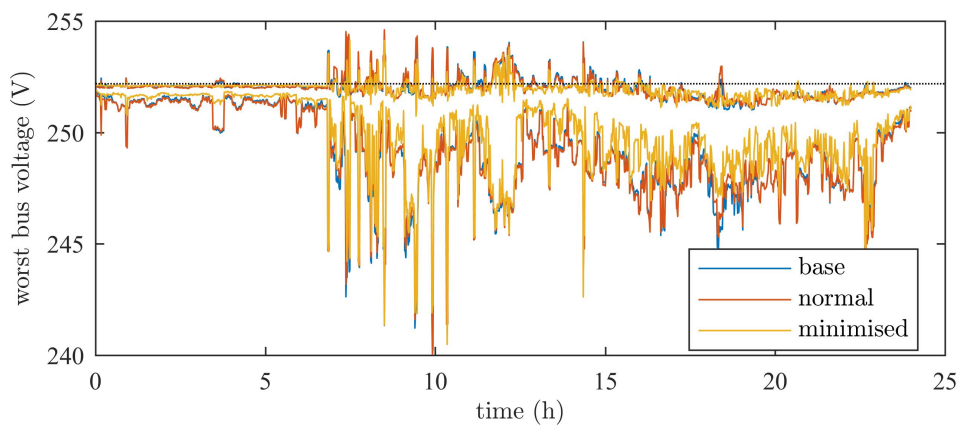
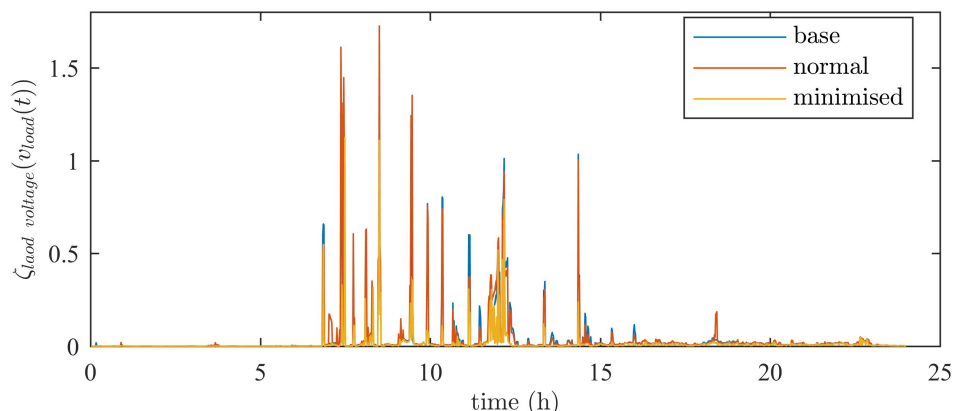


Figure A.2: Additional ESMU voltage level comparison between base, normal and the case where the ESMU's schedule was adjusted.

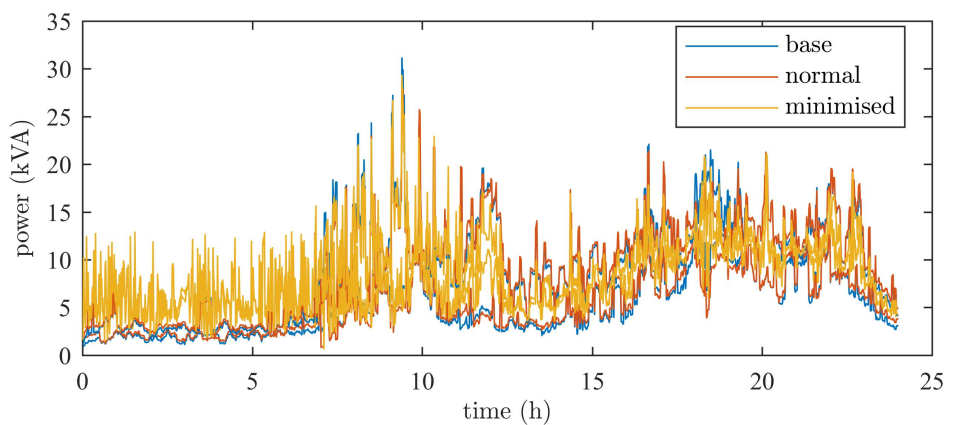


(a) Highest and lowest voltage levels in entire network

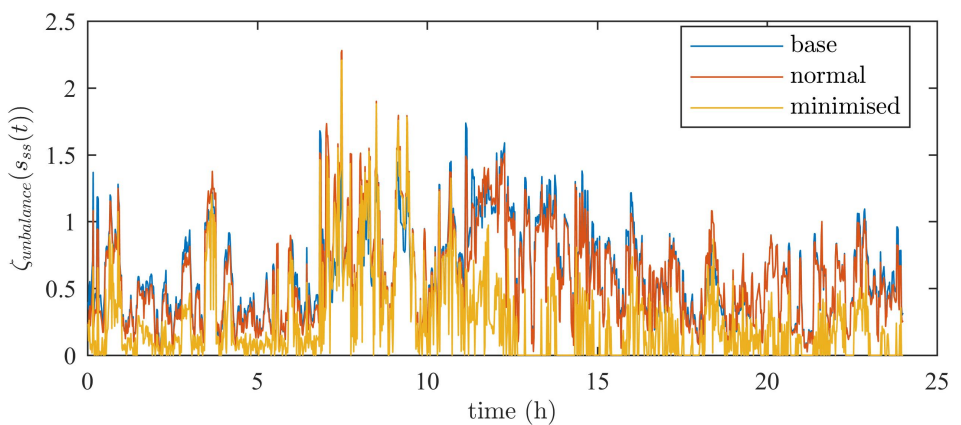


(b) Cost associated with highest and lowest voltage levels in entire network

Figure A.3: Additional voltage level comparison between base, normal and the case where the ESMU's schedule was adjusted.



(a) Highest and lowest phase power



(b) Phase unbalance cost

Figure A.4: Additional phase unbalance cost comparison between base, normal and the case where the ESMU's schedule was adjusted.

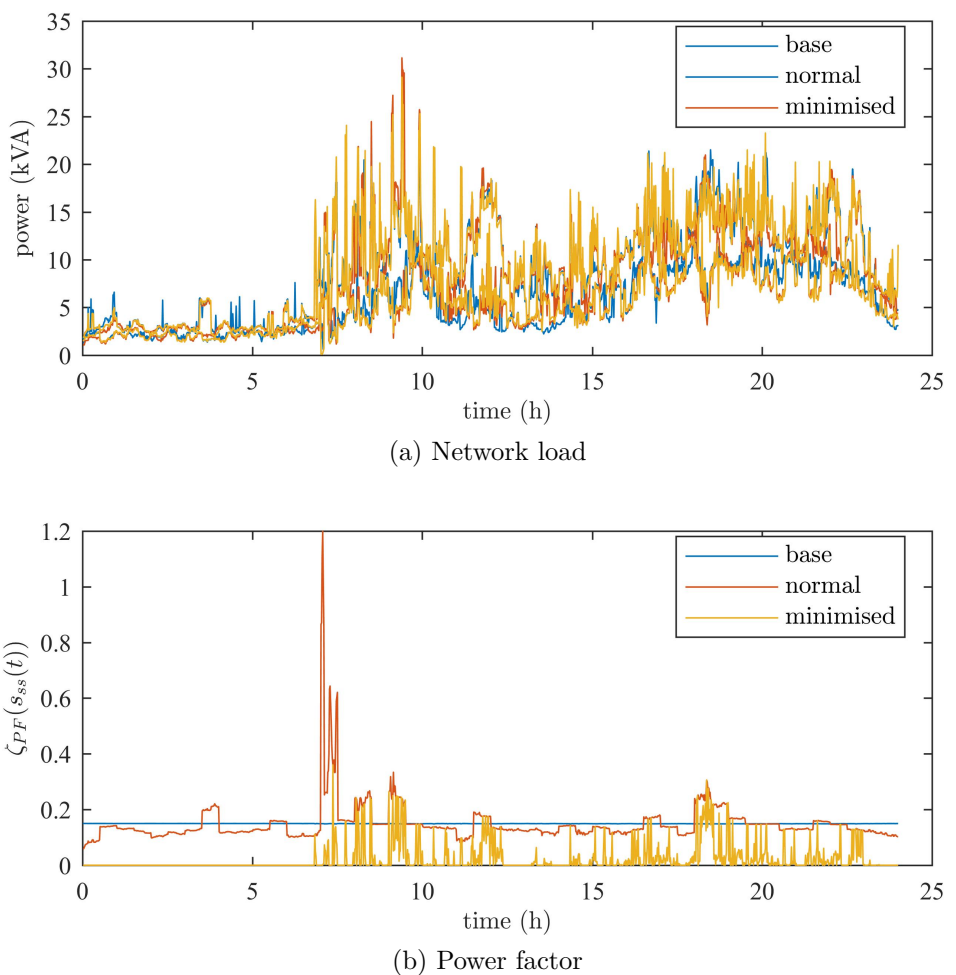
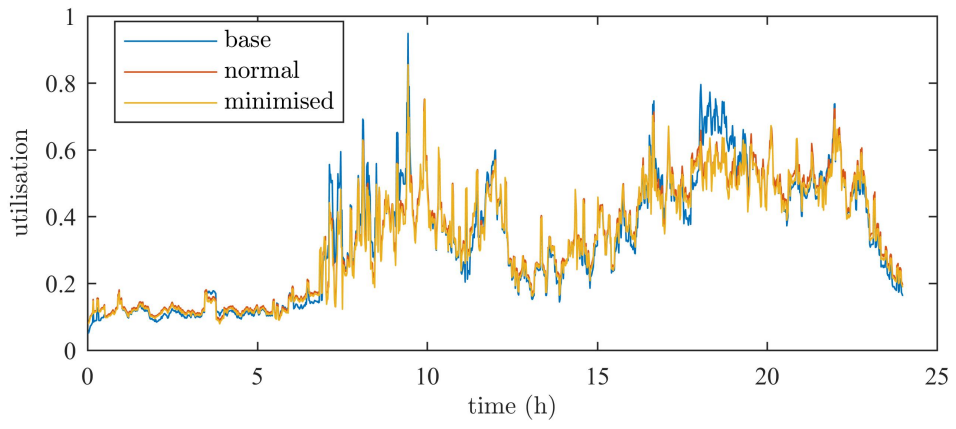
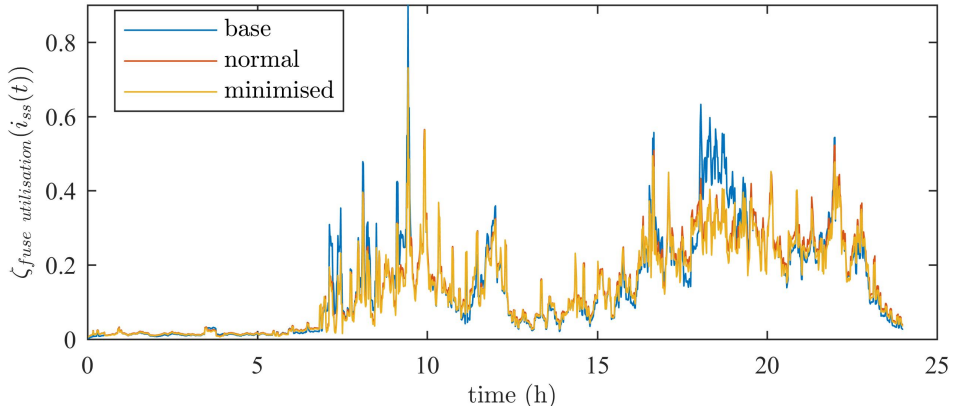


Figure A.5: Additional power factor cost comparison between base, normal and the case where the ESMU's schedule was adjusted.

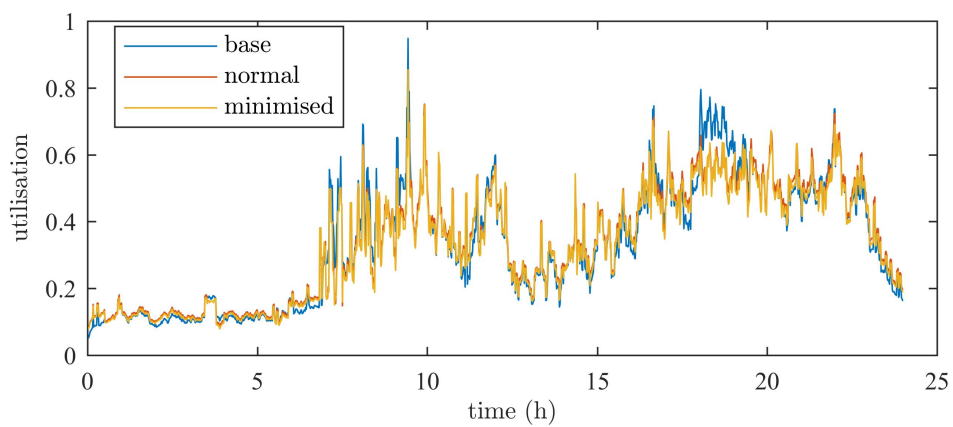


(a) Utilisation of the substation fuse

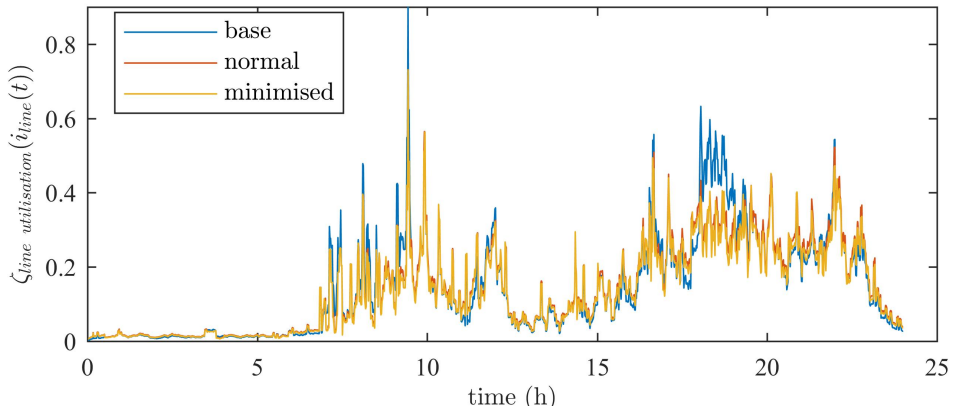


(b) Cost associated with the utilisation of the substation fuse

Figure A.6: Additional comparison of the substation fuse utilisation between base, normal and the case where the ESMU's schedule was adjusted.

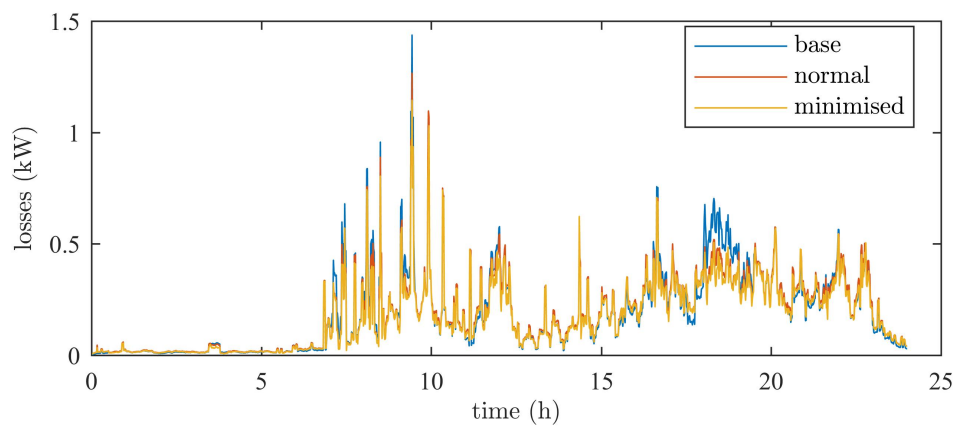


(a) The highest line utilisation of any line in the entire network

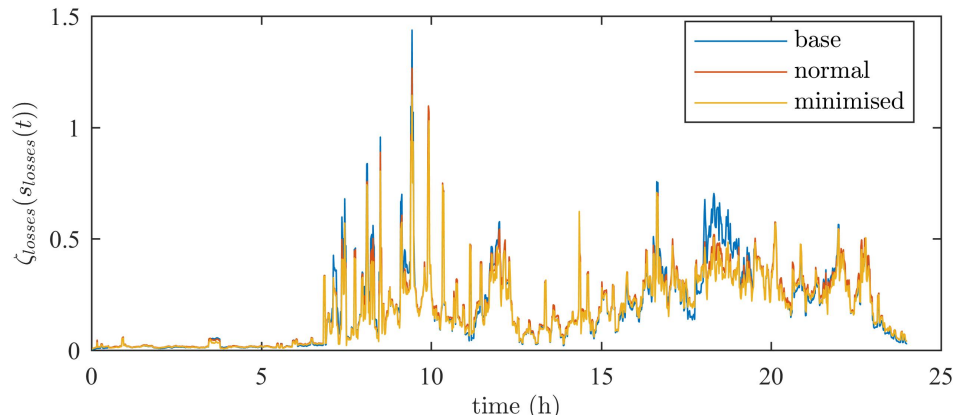


(b) The highest cost associated to the highest line utilisation of any line in the entire network

Figure A.7: Additional line utilisation comparison between base, normal and the case where the ESMU's schedule was adjusted.



(a) Distribution losses



(b) Cost associated to distribution losses

Figure A.8: Additional comparison of distribution loss cost between base, normal and the case where the ESMU's schedule was adjusted.

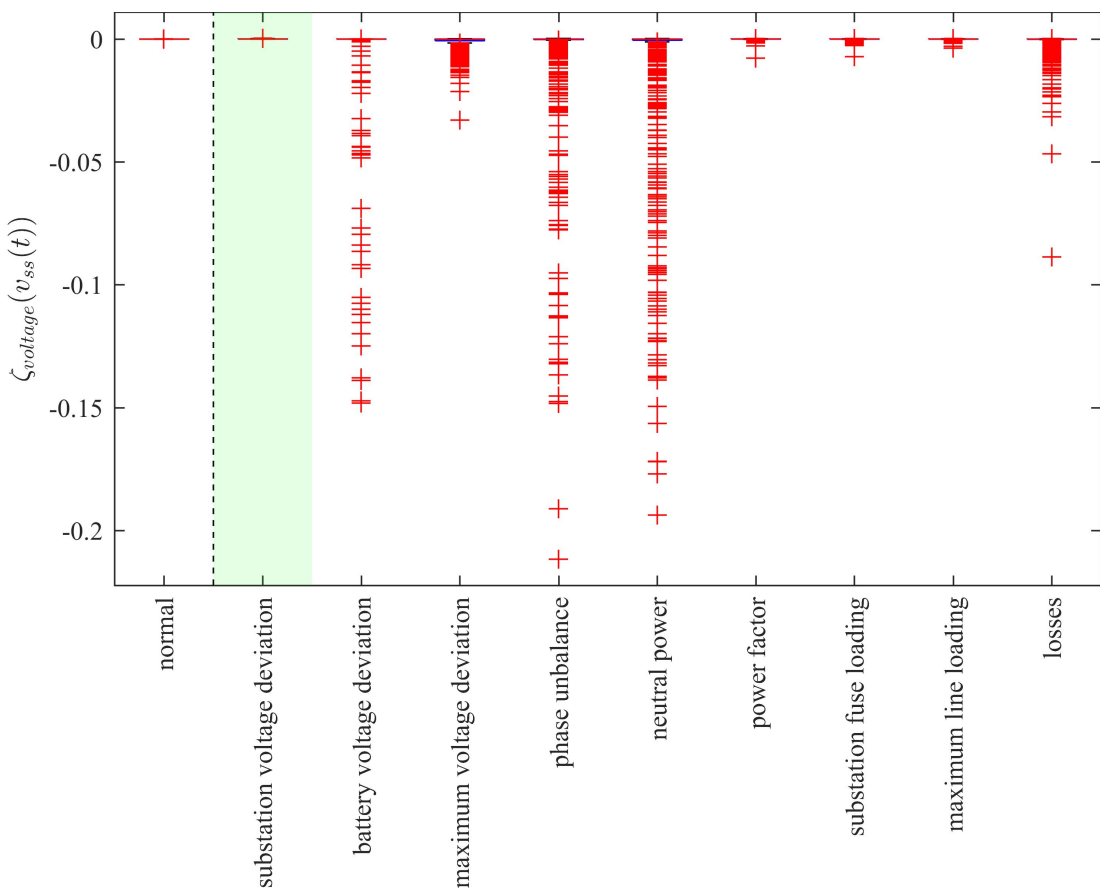


Figure A.9: Cost difference spread, based on the ESMU schedule adjustment to minimise substation voltage deviation

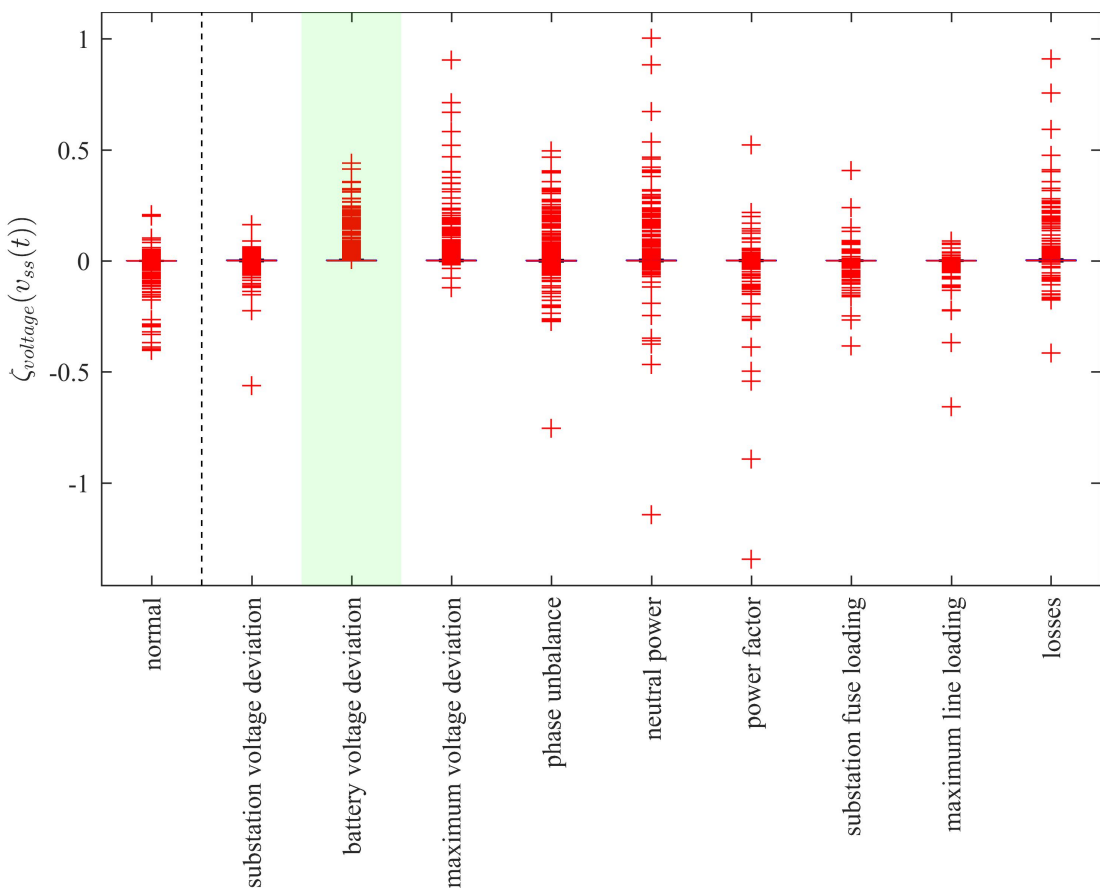


Figure A.10: Cost difference spread, based on the ESMU schedule adjustment to minimise ESMU's PCC voltage deviation

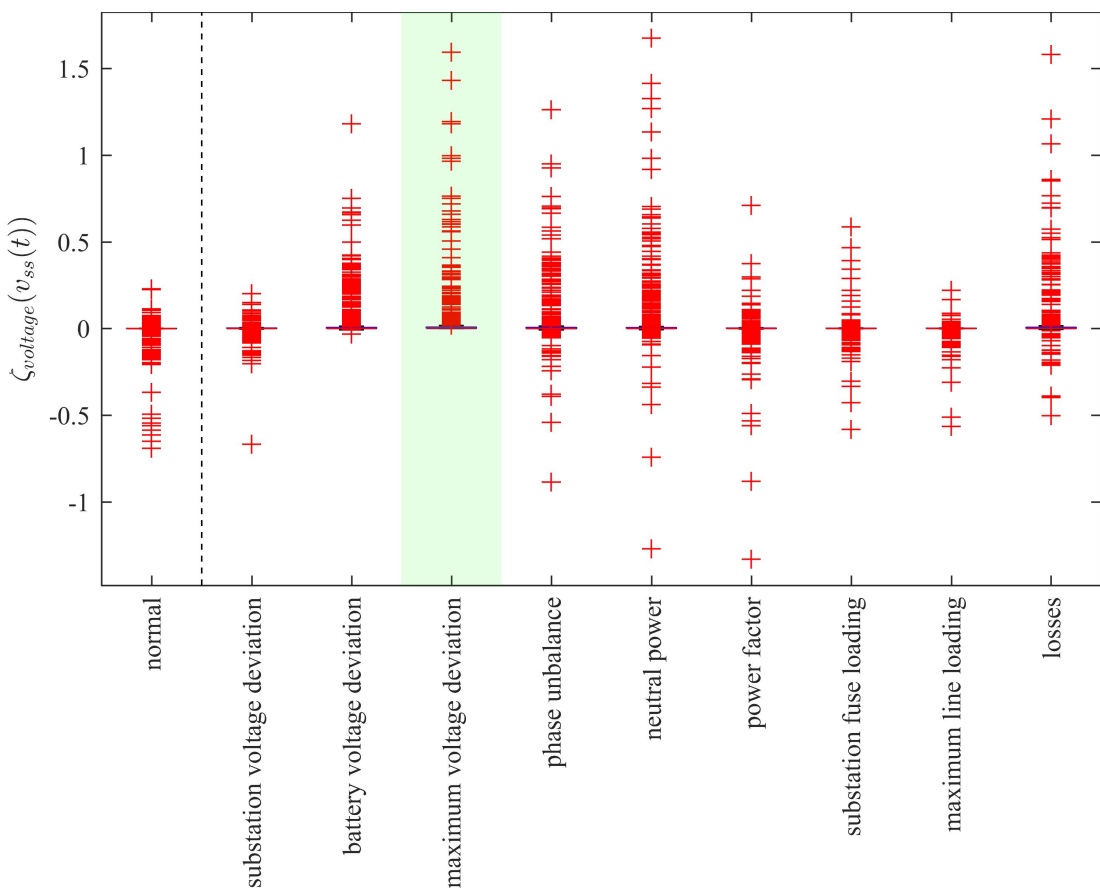


Figure A.11: Cost difference spread, based on the ESMU schedule adjustment to minimise the maximum voltage deviation on any bus of the network

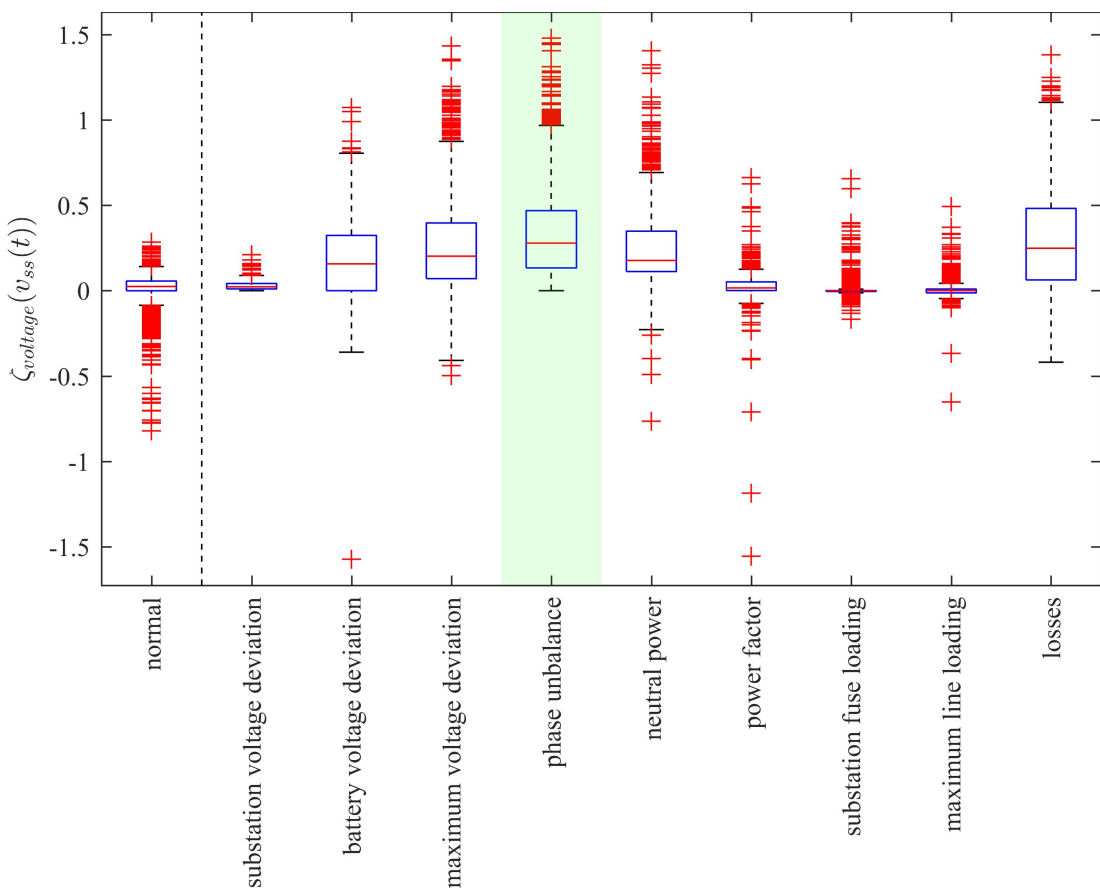


Figure A.12: Cost difference spread, based on the ESMU schedule adjustment to minimise the network's phase unbalance

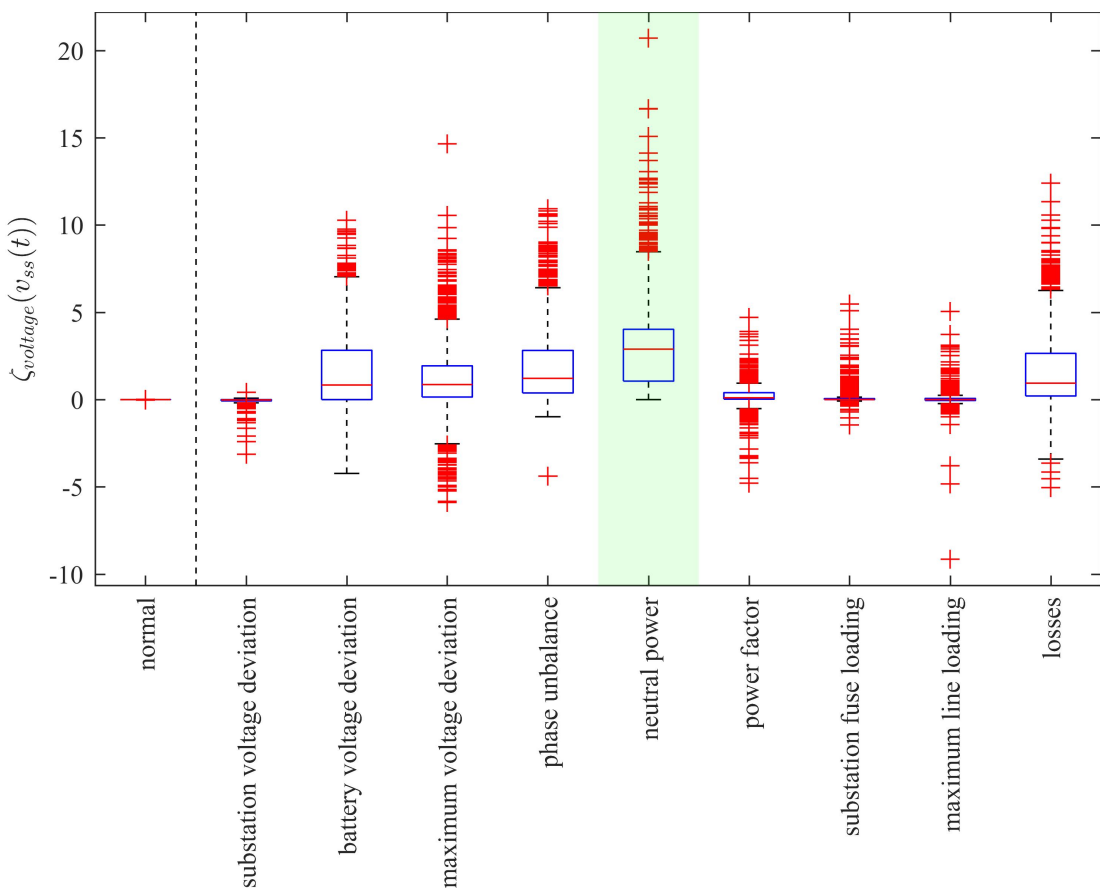


Figure A.13: Cost difference spread, based on the ESMU schedule adjustment to minimise the network's power flow in the neutral conductor

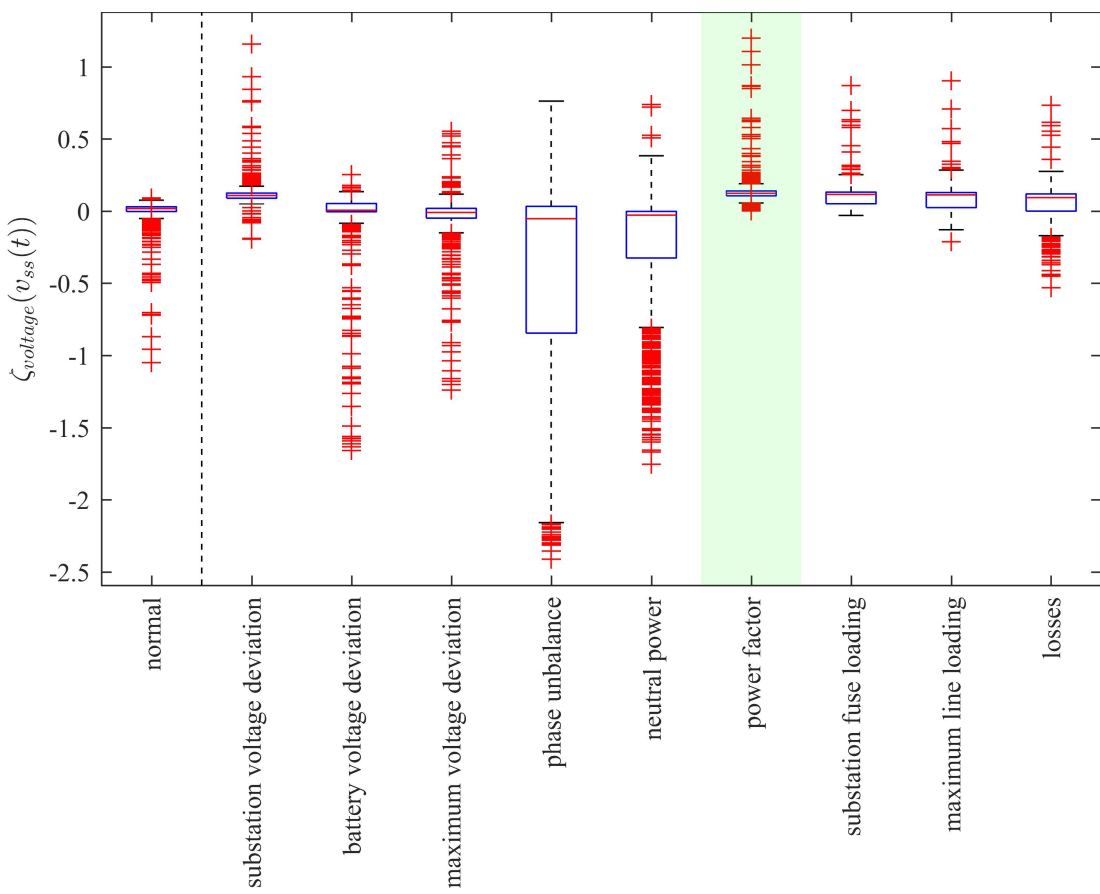


Figure A.14: Cost difference spread, based on the ESMU schedule adjustment to minimise the network's offset to unity power factor

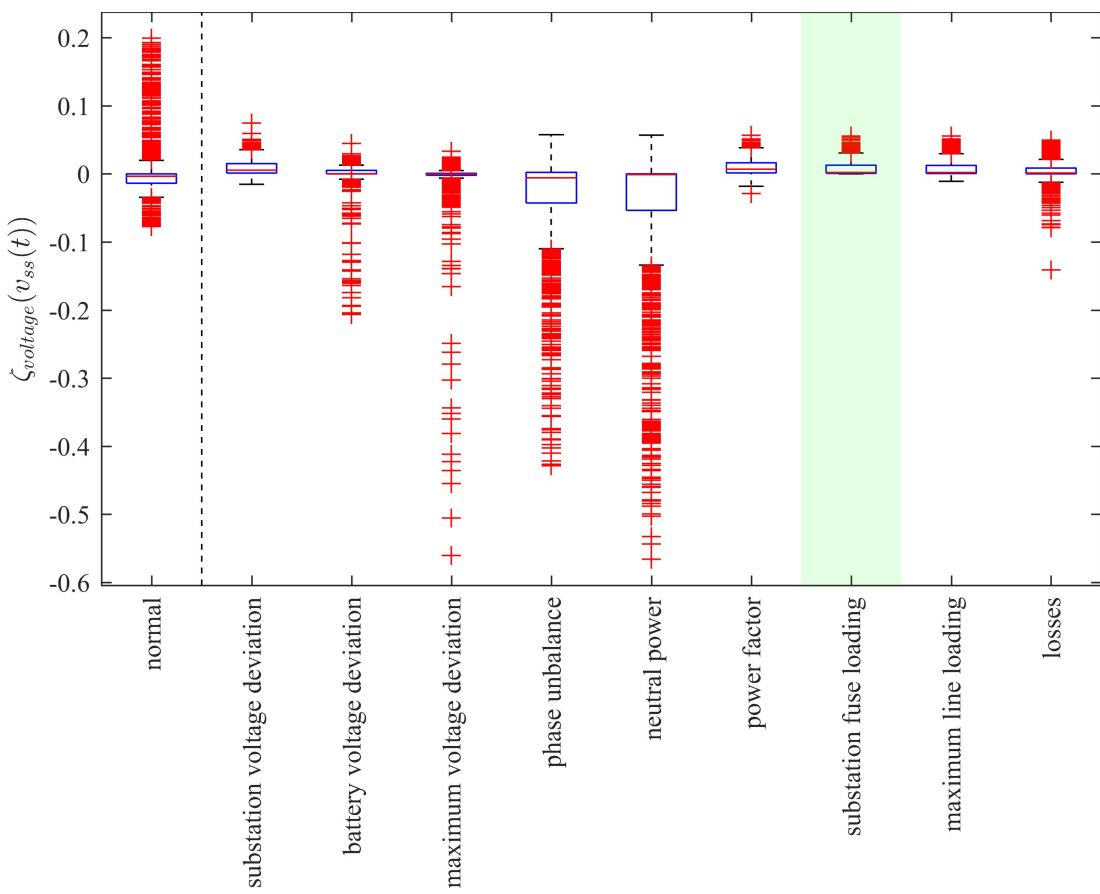


Figure A.15: Cost difference spread, based on the ESMU schedule adjustment to minimise the substation's fuse utilisation

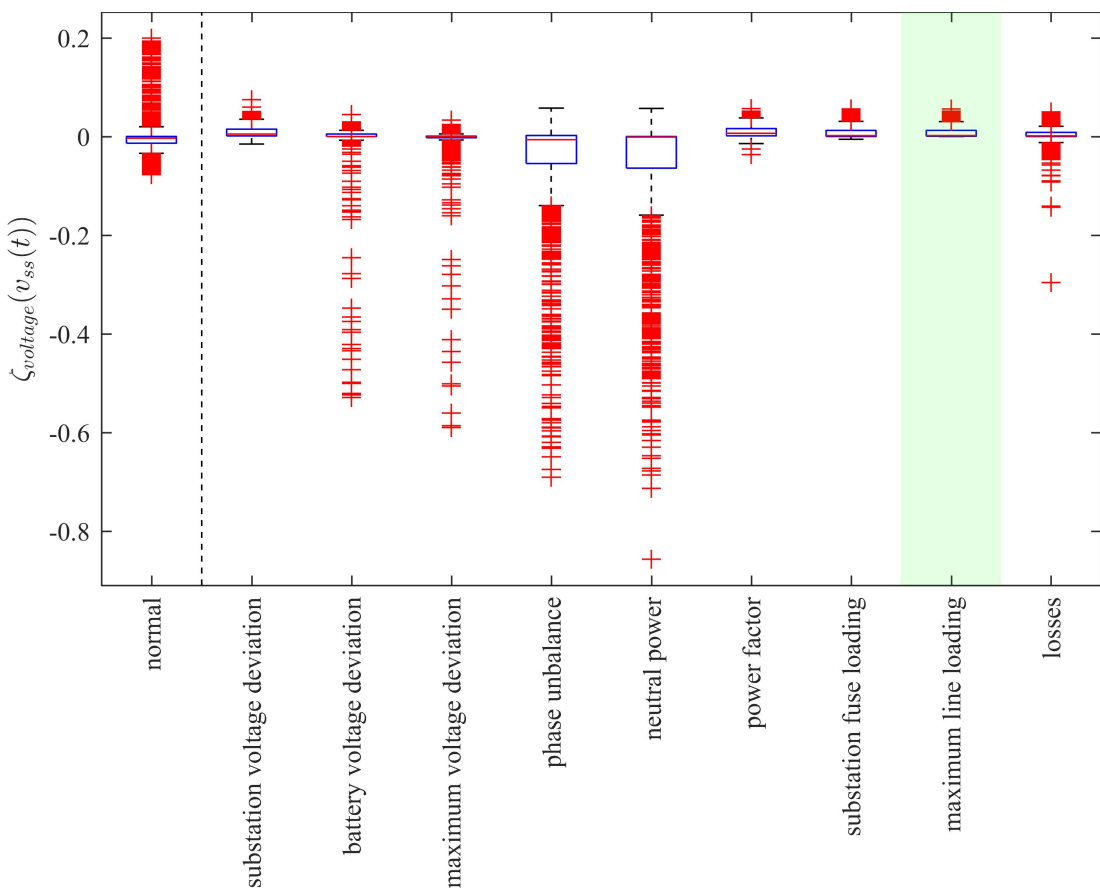


Figure A.16: Cost difference spread, based on the ESMU schedule adjustment to minimise the maximum line utilisation of any line in the network

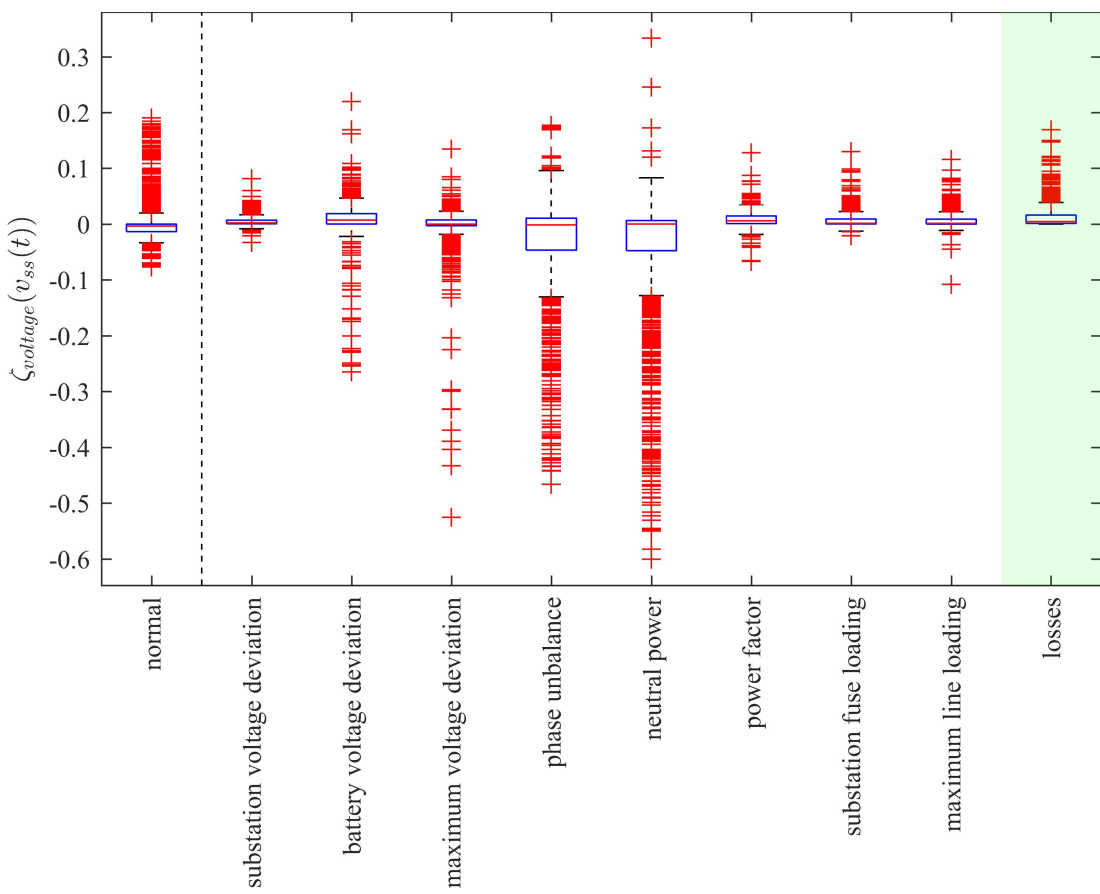


Figure A.17: Cost difference spread, based on the ESMU schedule adjustment to minimise distribution losses

Appendix B

Multi-Agent Systems

B.1 FIPA Implementation

B.2 Communication Protocols

Appendix C

Stochastic EV Demand Model

Appendix D

Network Simulation Interface

D.1 OpenDSS

D.2 Java

D.3 MATLAB

D.4 Python